Referee 1 - Anonymous

We thank the reviewer for the positive comments to this manuscript. Here we respond to specific comments point by point.

Comment 1:

Materials and methodology. Page 4, lines 115–116: "The method in Di Biagio et al. (2017), allowing for the realistic generation of dust aerosols from parent soils, was adopted for the dust particles generation." Page 4, lines 123–125: "CESAM (French acronym for Experimental Multiphasic Atmospheric Simulation Chamber), a 4.2 m3 stainless steel atmospheric simulation chamber (Wang et al., 2011), was used to generate the PM20 samples while acquiring information on the size distribution and the optical properties of the generated dust aerosols." Two different chambers were used to resuspend soils. Comment: The method in Di Biagio et al. (2017) allows for the realistic generation of dust aerosols from parent soils, how about CESAM? Are the physical and chemical characteristics of the sand and dust generated by these two chambers the same?

Response:

a) We are sorry for the confusion, Di Biagio et al. (2017) used CESAM to generate dust particles.

These paragraphs have been modified according to the referee's comments:

Line2 110-137: The PM_{10} samples were used for offline composition and mineralogy analyses. PM_{10} was collected using a custom-made reactor schematically represented in Figure S1. The method in Di Biagio et al. (2017) was adopted to generate dust particles, allowing for the realistic generation of dust aerosols from parent soils. Firstly, the sediment samples were sieved to < 1 mm to remove the non-erodible fraction. 15 g of sediments were placed in a Büchner flask and flushed with pure nitrogen for 10 minutes to eliminate gaseous contamination and residual water vapour. The sample was then shaken for 5 minutes at 70 Hz on a sieve shaker (Retsch AS200) and injected in a glass manifold of approximately 1 L by nitrogen gas at 10 L min^{-1}, while the air was pumped at a flow rate of 30 L min^{-1} into a PM_{10} sampling head (custom-made). The PM_{10} fraction was collected on 0.4 µm polycarbonate filters and transferred into centrifuge tubes. The system was manually cleaned prior to each loading and flushed for 5 minutes with pure nitrogen to ensure an initial particle-free environment.

The PM_{20} fraction was collected using the large-scale atmospheric simulation chamber, CESAM (French acronym for Experimental Multiphasic Atmospheric Simulation Chamber) (Wang et al., 2011). The CESAM simulation facility, made of stainless steel, consists in a 4.2 m^3 multi-instrumented environmental chamber which allows to measure the size distribution and the optical properties of the generated dust aerosols while collecting filter samples for offline analysis (Di Biagio et al., 2017; 2019). Dust particles were generated with the sieve shaker (Retsch AS200) using the same protocol as for the small reactor as in Di Biagio et al. (2017), and injected in the CESAM chamber by flushing a Büchner flask with nitrogen gas carrier at 10 L min^{-1} for 10 minutes. The dust aerosol injected in CESAM was left suspended for about 10 minutes to allow the particle mass concentration inside the chamber to become spatially uniform. Dust particles corresponding to approximately the PM_{20} fraction were extracted from the chamber using custom-made filter samplers as in Caponi et al. (2017). Particles were collected by filtration on 0.4-µm pore size polycarbonate filters of 37 mm diameter at 7 L min^{-1} for approximately 1 hour. The residence time of particles in the chamber depends on their size. As shown in Di Biagio et al. (2017), particles larger than 1 µm have a lifetime of 20-30 minutes, while the lifetime of particles smaller than 1 µm can exceed a day. A second filter sample was collected successively to the first one to verify if the chemical composition of the dust was dependent on size. No significant difference was observed (not shown). The relation between the composition, size distribution and optical properties of the aerosol dust will be the subject of a companion paper (Baldo et al., in preparation).

b) The PM_{10} resuspension apparatus was used to collect dust particles primarily to determine the chemical composition, mineralogy, and Fe speciation in the samples. The XRF measurements conducted on both the PM_{10} and PM_{20} fractions showed that these have very similar chemical composition. Page 9, line 165-268: "The XRF measurements showed that the difference between PM_{10} and PM_{20} in element oxide content > 1% including CaO, Fe_2O_3, Na_2O, MgO, Al_2O_3, SiO_2 and TiO_2 is within 16%. For Fe_2O_3, Al_2O_3, SiO_2 which are the major element oxides in the dust samples, the relative differences in content are <10%".

Comment 2:

Comparison of Icelandic dust with North African and Asian dust. Page 12, lines 357-359: "TiO_2 catalyses heterogeneous photochemical reactions of atmospheric trace gases including SO_2, NO_2, VOC and O_3, and contributes to the chemical balance of the atmosphere (Chen et al., 2012). In North African and Asian dust, TiO_2 is around 1% (e.g., Formenti et al., 2014b; Jeong, 2008; Shi et al., 2011b), which is significantly lower than that in Icelandic dust (2-5.5%)." Comment: Titanium dioxide (anatase and rutile) can serve as photocatalyst in oxidation and reduction reactions. However, TiO_2 given by XRF is not the mineral of TiO_2, but element Ti. The high content of element Ti in dust does not mean that it contains higher TiO_2 minerals.

Response:

This paragraph has been modified according to the referee's comments:

Lines 357-359: TiO_2 catalyses heterogeneous photochemical reactions of atmospheric trace gases including SO_2, NO_2, VOC and O_3, and contributes to the chemical balance of the atmosphere (Chen et al., 2012). In North African and Asian dust, TiO_2 is around 1% (e.g., Formenti et al., 2014; Jeong, 2008; Shi et al., 2011). In Icelandic dust, the element oxide concentration of Ti is relatively high 2-5.5%, although Ti can be not just as TiO_2 minerals (anatase and rutile). Ti may be present in magnetite and aluminosilicate minerals (e.g., augite) or in the amorphous glass.

Referee 2 – Kandler

General Response: We thank Dr. Kandler for providing constructive comments. We addressed each of the comments point by point below.

Comment 1:

Table 1: the shown CIA values don't agree with the formula given in line 185 and the oxide weights in the table. E.g., the CIA in the first line is 51. Recalculate. 385/390: Adjust the statements. Figure 7 + 8: Adjust the plot and in case conclusions.

Response:

Thank you for pointing this out. We apologize for making a mistake in the formula used to calculate the CIA. The CIA was calculated according to the formula in Price and Vebel 2003, thus the major element oxides are not as molar fractions but as molecular proportion of the element oxides. This has now been modified (Please see response to comment 3).

Comment 2:

186: How can the CIA defined the given way become larger than 100?

Response:

That was another mistake, 100 is the optimum weathered value.

Comment 3:

190: Please remove the comments related to PIA and CIW, as they don't seem to be used

Response:

The Chemical Weathering Index paragraph in the methodology section, lines 180-192, has been modified according to the referee's comments:

1.1 Chemical weathering index

The degree of chemical weathering of Icelandic dust was calculated based on the elemental composition. This is important to evaluate the presence in the samples of secondary minerals such as clays. The chemical index of alteration (CIA) (Nesbitt and Young, 1984) was considered most suitable for the present datasets based on the chemical compositions. The CIA is interpreted as a measure of the degree of weathering of aluminium silicate minerals, (in particular feldspars) into clay minerals. In this study, the CIA was calculated according to Price and Velbel (2003) using the molecular proportion of the element oxides which were obtained by dividing the weight percentage of each oxide by the molecular weight of the oxide:

$$\mathrm{CIA} = \frac{\mathrm{Al_2O_3}}{\mathrm{Al_2O_3} + \mathrm{CaO} + \mathrm{Na_2O} + \mathrm{K_2O}} \times 100$$

CIA ≤ 50 represents the optimum fresh value, while 100 is the optimum weathered value. The CIA uncertainty was estimated using the error propagation formula and is ~14%.

Comment 4:

140: Why was PM_{20} less than PM_{10}? That doesn't seem to be logical without further explanation.

Response:

We should have made this clearer, PM_{20} and PM_{10} samples were collected from two different chambers and with two different samplers (the flow rate also differs). The mass concentration in the two collection systems is considerably different. The PM_{20} fraction was collected using CESAM, a 4.2 m^3 stainless steel atmospheric simulation chamber at a flow rate of 7 L min^{-1}. In the dust resuspension apparatus PM_{10} is collected at a flow rate of 30 L min^{-1}, and the volume of the reactor is around 1 L.

Line 140 has been modified according to the referee's comments:

Line 140: PM_{20} samples were not analysed because the mass of dust particles collected from CESAM was not sufficient for the XRD analysis. This is because the mass concentrations in the CESAM chamber is much lower compared to the custom-made reactor for the PM_{10} collection.

Comment 5:

150-152: How can a mineral (augite) be chosen as reference for an amorphous matter in XRD?

Response:

In this study, the chemical composition of the glass fraction in the Icelandic dust samples is unknown. However, the samples MIR45 is mostly amorphous, and showed similar chemical composition to augite. In our method, we consider the amorphous phase as the augite phase but with poor crystallinity. To support our choice, we observed that the main diffraction peak for the augite phase was at the same position as the amorphous contribution in the diffractograms. In practice, the mineral phase of augite identified using the Highscore Plus 3.0 software was modified in MAUD to amorphous phase by broadening its diffraction peaks following the method in Lutterotti et al. (1998), and saved as reference.

Comment 6:

Table 2: Why was the uncertainty for anorthite calculated differently? Why is the chi square for H55 so much higher? Apparently the spectrum fit was worse – missing minerals?

Response:

Page 5, line 152: "The Rietveld model refines n -1 phases. As the total is fixed to100, the last phase results from the subtraction of the sum of the n refined phases". In this study, using the MAUD software, for all the samples the anorthite phase results from the subtraction of the sum of the other refined phases. Since the weight ratio of the anorthite phase are not refined, the corresponding uncertainty is not calculated by the software. Thus, the uncertainty for anorthite were calculated using the error propagation formula.

The higher chi square values obtained for the samples H55 may be mainly due to missing mineral phases. X-Ray Diffraction (XRD) is a global analysis that requires a minimum number of crystals for each phase, so phases which are less than about 2 or 3 wt.% may not be characterized by XRD. It can be difficult to clearly distinguish minor phases because of wide and overlapping peaks and low diffraction intensity. In addition, when the chi square is close to one, there is no guarantee that the model is correct. In particular, when a large percentage of the intensity comes from the background, this can give relatively small chi square values (Toby, 2006). Thus, "in this study, the quality of the fitting was evaluated considering the chi square, and by comparing visually the observed and calculated diffractograms to obtain a realistic chemical model (Toby, 2006)", Page 5, lines 154-156. H55 is the most crystalline sample and compared to the other samples having chi square values very close to one, its diffraction intensities are considerably higher than the background signal. Lines 154-157 have been modified to highlight this:

Lines 154-157: The quality of the fitting was evaluated considering the χ^2 calculated by the model close to one, and by comparing visually the observed and calculated diffractograms to achieve a realistic chemical model (Toby, 2006). Small χ^2 values can be obtained when a large percentage of the intensity comes from the background (Toby, 2006). For example, the estimated χ^2 for H55 is relatively high (2.3-3.8) primarily due to missing minor mineral phases. However, H55 has the lowest fraction of amorphous material and compared to the other samples having χ^2 values very close to one, its diffraction intensities are considerably higher than the background signal.

Comment 7:

332-333: While the fractionation is surely lower than the one observed in the hot deserts, at least for the H55 there is some with respect to microcline and glass. Maybe because Hagarvatn is a lake and might have longer residence time of sediments, similar to the hot desert hot spots?

Response:

Yes, there is some fractionation in H55. Actually, the Hagavatn sediments are reworked materials from crystalline lava that were previously (at least partly) on the surface. The glacier advanced over the lava, abraded it, and subsequently retreated. Other samples are almost entirely derived from glacial abrasion of hyaloclastic materials, thus being more "uniform" and having much smaller crystalline component. Line 332 has been modified to highlight this:

Line 332: Mineralogical fractionation is not evident in Icelandic dust, probably due to the low chemical weathering, and the lack of larger mineral grains such as quartz, K-feldspar, and clays. Only the more crystalline samples from Hagavatn showed some fractionation with respect to K-feldspar and glass, while the sediments from the other sites are derived from the glacial abrasion of hyaloclastite and thus, they tend to be more uniform.

Comment 8:

171-175: XRF determined elements. Why is oxide weight calculated, if iron content then is back-transformed from the oxide weights? Apart from that, is Fe_2O_3 a reasonable assumption for Icelandic dust?

Response:

Yes, XRF determines elements. It is a common practice to calculate the oxide weight in geoscience (Formenti et al., 2014; Formenti et al., 2011; Lafon et al., 2006; Linke et al., 2006). This allows a better estimate of the dust mass and in reality, oxygen is always associated with these elements. We recognize that some Fe may be as FeO but XRF does not distinguish Fe(II) or Fe(III). We added a sentence to explain why we used Fe_2O_3 and also clarify the potential presence of FeO that we did not consider:

Lines 173-175: The total mass on filter was calculated as the sum of the mass of the oxides of the major crustal elements reported in Table 1. Fe is assumed to be as Fe_2O_3. We recognize that Fe(II) and Fe(III) can be found in the mineral phases (e.g., magnetite, augite) and in the amorphous glass, but the Fe(II)/Fe(III) ratio is not known.

Comment 9:

357-359: The photochemical activity is commonly described for rutile. But this is not identified by XRD, instead titanomagnetite is found. Also, the glass phase could contain considerable amounts of Ti, as the titanomagnetite contents doesn't seem to explain the total TiO2 content. Therefore, the conclusion here doesn't appear to be sound.

Response: (same response as to the second comment of referee 1)

This paragraph has been modified according to the referee's comments:

TiO_2 catalyses heterogeneous photochemical reactions of atmospheric trace gases including SO_2, NO_2, VOC and O_3, and contributes to the chemical balance of the atmosphere (Chen et al., 2012). In North African and Asian dust, TiO_2 is around 1% (e.g., Formenti et al., 2014; Jeong, 2008; Shi et al., 2011). In Icelandic dust, the element oxide concentration of Ti is relatively high 2-5.5%, although Ti can be not just as TiO_2 minerals (anatase and rutile). Ti may be present in magnetite and aluminosilicate minerals (e.g., augite) or in the amorphous glass.

Comment 10:

506-510: The conclusions refer to magnetite, but mainly titanomagnetite was identified. Is there anything known about the optical (and also Fe dissolution) properties of the latter?

Response:

Titanomagnetite ($Fe_{3-x}Ti_xO_4$) forms a complete solid solution series between the end-members magnetite (Fe_3O_4) and ulvöspinel (Fe_2TiO_4). Hettiarachchi et al. (2019) observed that there is a strong correlation between the Fe solubility and the Ti/Fe ratio, which suggests that the presence of Ti in magnetite can enhance its solubility.

Currently, there is limited knowledge of the optical properties of titanomagnetite minerals. Both magnetite and ulvöspinel strongly absorbs light throughout the UV-Vis region, although they may have different spectral features (e.g., the absorption peak in ulvöspinel is shifted from 300 nm to 500 nm) (Strens and Wood, 1979). The spectral feature of minerals of the titanomagnetite series may also depend on the Ti/Fe ratio.

Corrections

72: Check the spellings of Möller/Moller/Moeller. They have the same name (Möller)

85: Check the references. E.g., Urupina is not in the list.

93: Dust source areas?

167-170: That can be removed, as creation of defined standards is not topic.

Response:

All the corrections have been applied in the text. Changes in the references are highlighted in yellow in the revised manuscript. The correct spelling of all the Icelandic names has also been checked.

References

Caponi, L., Formenti, P., Massabo, D., Di Biagio, C., Cazaunau, M., Pangui, E., Chevaillier, S., Landrot, G., Andreae, M. O., Kandler, K., Piketh, S., Saeed, T., Seibert, D., Williams, E., Balkanski, Y., Prati, P., and Doussin, J. F.: Spectral- and size-resolved mass absorption efficiency of mineral dust aerosols in the shortwave spectrum: a simulation chamber study, Atmospheric Chemistry and Physics, 17, 7175-7191, doi: 10.5194/acp-17-7175-2017, 2017.

Chen, H., Nanayakkara, C. E., and Grassian, V. H.: Titanium dioxide photocatalysis in atmospheric chemistry, Chemical Reviews, 112, 5919-5948, doi: 10.1021/cr3002092, 2012.

Di Biagio, C., Formenti, P., Balkanski, Y., Caponi, L., Cazaunau, M., Pangui, E., Journet, E., Nowak, S., Caquineau, S., Andreae, M. O., Kandler, K., Saeed, T., Piketh, S., Seibert, D., Williams, E., and Doussin, J. F.: Global scale variability of the mineral dust long-wave refractive index: a new dataset of in situ measurements for climate modeling and remote sensing, Atmospheric Chemistry and Physics, 17, 1901-1929, doi: 10.5194/acp-17-1901-2017, 2017.

Di Biagio, C., Formenti, P., Balkanski, Y., Caponi, L., Cazaunau, M., Pangui, E., Journet, E., Nowak, S., Andreae, M. O., Kandler, K., Saeed, T., Piketh, S., Seibert, D., Williams, E., and Doussin, J. F.: Complex refractive indices and single-scattering albedo of global dust aerosols in the shortwave spectrum and relationship to size and iron content, Atmospheric Chemistry and Physics, 19, 15503-15531, doi: 10.5194/acp-19-15503-2019, 2019.

Formenti, P., Schutz, L., Balkanski, Y., Desboeufs, K., Ebert, M., Kandler, K., Petzold, A., Scheuvens, D., Weinbruch, S., and Zhang, D.: Recent progress in understanding physical and chemical properties of African and Asian mineral dust, Atmospheric Chemistry and Physics, 11, 8231-8256, doi: 10.5194/acp-11-8231-2011, 2011.

Formenti, P., Caquineau, S., Desboeufs, K., Klaver, A., Chevaillier, S., Journet, E., and Rajot, J. L.: Mapping the physico-chemical properties of mineral dust in western Africa: mineralogical composition, Atmospheric Chemistry and Physics, 14, 10663-10686, doi: 10.5194/acp-14-10663-2014, 2014.

Hettiarachchi, E., Reynolds, R. L., Goldstein, H. L., Moskowitz, B., and Rubasinghege, G.: Bioavailable iron production in airborne mineral dust:Control by chemical composition and solar flux, Atmospheric Environment, 205, 90-102, doi: 10.1016/j.atmosenv.2019.02.037, 2019.

Jeong, G. Y.: Bulk and single-particle mineralogy of Asian dust and a comparison with its source soils, Journal of Geophysical Research-Atmospheres, 113, doi: 10.1029/2007jd008606, 2008.

Lafon, S., Sokolik, I. N., Rajot, J. L., Caquineau, S., and Gaudichet, A.: Characterization of iron oxides in mineral dust aerosols: Implications for light absorption, Journal of Geophysical Research-Atmospheres, 111, doi: 10.1029/2005jd007016, 2006.

Linke, C., Möhler, O., Veres, A., Mohacsi, A., Bozóki, Z., Szabó, G., and Schnaiter, M.: Optical properties and mineralogical composition of different Saharan mineral dust samples: a laboratory study, 2006.

Lutterotti, L., Ceccato, R., Dal Maschio, R., and Pagani, E.: Quantitative analysis of silicate glass in ceramic materials by the Rietveld method, Materials Science Forum, 278, 87-92, 1998.

Nesbitt, H. W., and Young, G. M.: Prediction of some weathering trends of plutonic and volcanic-rocks based on thermodynamic and kinetic considerations, Geochimica Et Cosmochimica Acta, 48, 1523-1534, doi: 10.1016/0016-7037(84)90408-3, 1984.

Price, J. R., and Velbel, M. A.: Chemical weathering indices applied to weathering profiles developed on heterogeneous felsic metamorphic parent rocks, Chemical Geology, 202, 397-416, doi: 10.1016/j.chemgeo.2002.11.001, 2003.

Shi, Z., Krom, M. D., Bonneville, S., Baker, A. R., Bristow, C., Drake, N., Mann, G., Carslaw, K., McQuaid, J. B., Jickells, T., and Benning, L. G.: Influence of chemical weathering and aging of iron oxides on the potential iron solubility of Saharan dust during simulated atmospheric processing, Global Biogeochemical Cycles, 25, doi: 10.1029/2010gb003837, 2011.

Strens, R., and Wood, B.: Diffuse reflectance spectra and optical properties of some iron and titanium oxides and oxyhydroxides, Mineralogical Magazine, 43, 347-354, 1979.

Toby, B. H.: R factors in Rietveld analysis: How good is good enough?, Powder diffraction, 21, 67-70, doi: 10.1154/1.2179804, 2006.

Wang, J., Doussin, J. F., Perrier, S., Perraudin, E., Katrib, Y., Pangui, E., and Picquet-Varrault, B.: Design of a new multi-phase experimental simulation chamber for atmospheric photosmog, aerosol and cloud chemistry research, Atmospheric Measurement Techniques, 4, 2465-2494, doi: 10.5194/amt-4-2465-2011, 2011.

Distinct chemical and mineralogical composition of Icelandic dust compared to North African and Asian dust

Clarissa Baldo[1], Paola Formenti[2], Sophie Nowak[3], Servanne Chevaillier[2], Mathieu Cazaunau[2], Edouard Pangui[2], Claudia Di Biagio[2], Jean-Francois Doussin[2], Konstantin Ignatyev[4], Pavla Dagsson-Waldhauserova[5,6], Olafur Arnalds[5], A. Robert MacKenzie[1], Zongbo Shi[1]

[1]School of Geography Earth and Environmental Sciences, University of Birmingham, Birmingham, United Kingdom
[2]LISA, UMR CNRS 7583, Université Paris-Est-Créteil, Université de Paris, Institut Pierre Simon Laplace (IPSL), Créteil, France
[3]Plateforme RX UFR de chimie, Université de Paris, Paris, France
[4]Diamond Light Source, Didcot, Oxfordshire, UK
[5]Agricultural University of Iceland, Keldnaholt, Reykjavik, Iceland
[6]Faculty of Environmental Sciences, Czech University of Life Sciences, Prague, Czech Republic

Correspondence to: Zongbo Shi (z.shi@bham.ac.uk)

Abstract. Iceland is a highly active source of natural dust. Icelandic dust has the potential to affect directly the climate via dust-radiation interaction, and indirectly via dust-cloud interaction, snow/ice albedo effect and impacts on biogeochemical cycles. The impacts of Icelandic dust depend on its mineralogical and chemical composition. However, lack of data has prevented an accurate assessment of the role of Icelandic dust in the Earth system. Here, we collected surface sediment samples from five major Icelandic dust hotspots. Dust aerosols were generated and suspended in atmospheric chambers, and PM_{10} and PM_{20} fractions were collected for further analysis. We found that the dust samples primarily consist of amorphous basaltic material ranging from 8 wt% (from the Hagavatn hotspot) to 60-90 wt% (other hotspots). Samples had relatively high total Fe content (10-13 wt%). Sequential extraction of Fe to determine its chemical form shows that dithionite Fe (Fe oxides such as hematite and goethite) and ascorbate Fe (amorphous Fe) contribute respectively 1-6%, and 0.3-1.4% of the total Fe in Icelandic dust. The magnetite fraction is 7-15% of total Fe and 1-2 wt% of PM_{10}, which is orders of magnitude higher than in mineral dust from North Africa. Nevertheless, about 80-90% of the Fe is contained in pyroxene and amorphous glass. The initial Fe solubility (ammonium acetate extraction at pH 4.7) is from 0.08-0.6%, which is comparable to low latitude dust such as that from North Africa. The Fe solubility at low pH (i.e., 2) is significantly higher than typical low latitude dust (up to 30% at pH 2 after 72 hrs). Our results revealed the fundamental differences in composition and mineralogy of Icelandic dust from low latitude dust. We attribute these differences to the low degree of chemical weathering, the basaltic composition of the parent sediments, and glacial processes. Icelandic dust contributes to the atmospheric deposition of soluble Fe and can impact primary productivity in the North Atlantic Ocean. The distinct chemical and mineralogical composition, particularly the high magnetite content (1-2 wt%), indicates a potentially significant impact of Icelandic dust on the radiation balance in the sub-polar and polar regions.

1 Introduction

Airborne mineral dust has a major influence on the global climate. Depending on the chemical and mineralogical dust composition (together with the size distribution and shape), dust particles affect the radiation balance by scattering and absorbing the solar radiation, and by scattering, absorbing, and re-emitting terrestrial radiations (e.g., Haywood et al., 2003; Sokolik and Toon, 1999). This can produce cooling or warming of the atmosphere, and consequently alter the atmospheric circulation, stability, and cloud cover (e.g., Arimoto, 2001; Carslaw et al., 2010; Choobari et al., 2014; Maher et al., 2010). Dust can also act as cloud condensation and ice nuclei, influencing cloud properties and lifetime (e.g., Tang et al., 2016; Atkinson et al., 2013). In the cryosphere, dust deposition on snow and ice reduces the surface albedo, altering snow melting rate (e.g.,Dumont et al., 2014; Meinander et al., 2014; Peltoniemi et al., 2015; Qian et al., 2015). Finally, dust can also affect the biogeochemical cycles of terrestrial and marine ecosystems by deposition of nutrients and pollutants (e.g., Jickells and Moore, 2015; Jickells et al., 2005; Kanakidou et al., 2018; Mahowald et al., 2010; Shi et al., 2012; Stockdale et al., 2016).

Natural dust is emitted from soil surfaces through wind erosion and is generally associated with desert dust from arid and semiarid regions. However, significant dust events occur also in cold regions at high latitude (Bullard et al., 2016). In the Northern hemisphere, high latitude (>60°N) dust sources includes for example Alaska, Canada, Greenland, and Iceland, and contributes about 3% of global dust emissions (Groot Zwaaftink et al., 2016).

Iceland is among the most active dust source areas in the world. Iceland has extensive sandy deserts subjected to intense aeolian processes (Arnalds et al., 2001).The active aeolian areas cover 15,000 km^2 and include super active dust hotspots. These areas have the potential to generate millions of tonnes of dust during major dust storm events (Arnalds et al., 2016). Iceland experiences 34-135 dust events per year, which is comparable to dust-active area in arid regions including North Africa and China (Dagsson-Waldhauserova et al., 2014a). The dust can travel long distance and reach Europe and the high Artic (Baddock et al., 2017; Moroni et al., 2018; Dordevic et al., 2019; Prospero et al., 2012; Groot Zwaaftink et al., 2017; Groot Zwaaftink et al., 2016).

Iceland lies in the North Atlantic Ocean, just south of the Arctic Circle. Iceland is a volcanic hotspot along the northern end of the Mid-Atlantic ridge and has intensive volcanic activity (Oskarsson, 1980). Around 10% of Iceland is covered by glaciers (Björnsson and Palsson, 2008). Volcanic activity within glaciers is common in Iceland (Jakobsson and Gudmundsson, 2008). Glacial flood plains contain fine glacial volcanic sediments that supply the Icelandic dust hotspots (Jensen et al., 2018; Arnalds, 2010; Arnalds et al., 2016). Sandy areas in Iceland have a dark surface and are often dominated by amorphous basaltic glass (Arnalds et al., 2001). Therefore, Icelandic cold deserts are different from deserts in arid continental areas such as Africa and Asia.

Arnalds et al. (2014) estimated that 30-40 Tg of Icelandic dust are deposited annually on land, glaciers and sea. The majority is deposited on land, and around 18-35% reach the ocean. Icelandic dust can affect the climate via dust deposition on glaciers. Wittmann et al. (2017) observed that the deposition of small amounts of dust on the Vatnajökull, the largest ice cap in Iceland, caused a positive radiative effect and enhanced the ice melting due to the reduced surface albedo. Outdoor experiments found that thin layers of volcanic deposits on the Vatnajökull ice cap accelerated snow melting as a result of the reduced surface albedo, while thick layers of volcanic deposits (1.5-15mm) had insulating effects because of reduced heat conduction to the glacier surface (Dragosics et al., 2016; Möller et al., 2018; Möller et al., 2016). The Soot on the Snow experiments in 2013 investigated the effect of black carbon (BC) and volcanic sand deposited on snow (Meinander et al., 2014; Peltoniemi et al., 2015). The results showed that the volcanic sand from Iceland reduces the surface albedo and increases the melting rate of snow similarly to black carbon. Icelandic dust has strong absorption capacity (Zubko et al., 2019). Indeed, Icelandic dust is also rich in iron (Fe) (e.g., Arnalds et al., 2014). The Fe speciation regulates the light absorption properties of mineral dust in the shortwave spectrum, as Fe oxide minerals strongly absorb the solar radiation (Caponi et al., 2017; Derimian et al., 2008; Di Biagio et al., 2019; Engelbrecht et al., 2016; Formenti et al., 2014a; Lafon et al., 2006; Moosmuller et al., 2012; Sokolik and Toon, 1999). In addition, atmospheric deposition of soluble Fe to the ocean can stimulate primary productivity and enhance the carbon uptake, consequently affecting the carbon budget and climate (e.g., Jickells et al., 2005). As a consequence, Icelandic dust contributes to the instantaneous radiative forcing (IRD) in the Artic (Kylling et al., 2018), and may influence the biogeochemical processes in the sub polar North Atlantic Ocean, which is seasonally Fe limited (Arnalds et al., 2014).

Icelandic dust scavenges effectively SO_2 and can possibly participate in a variety of heterogeneous reactions in the atmosphere, and thus influence the chemical balance of the atmosphere (Urupina et al., 2019). Icelandic dust is also a potential source of ice nucleating particles (Paramonov et al., 2018). The increase in ice nucleating particles may shorter the lifetime and lower the albedo of mixed-phase clouds (Vergara-Temprado et al., 2018), which have a significant impact on the energy budgets in the Arctic region (Boucher et al., 2013).

However, our knowledge on the chemical and mineralogical composition of Icelandic dust is very limited, which prevents us to provide a more realistic estimation on their local and regional impacts.

Here we determine the chemical and mineralogical composition of Icelandic dust from major dust ~~plume~~ source areas. In particular, we focus on the Fe speciation as it determines the light-absorption properties in the shortwave spectrum. The fractional Fe solubility of Icelandic dust is also determined. The Icelandic dust composition and Fe solubility are compared to North African and Asian dust. The potential direct radiative effect and the implications for the primary productivity in the North Atlantic Ocean are also discussed.

2 Materials and methodology

2.1 Sample collection and experimental setup

Surface sediment samples were collected from five major dust hotspots in Iceland: D3 (Dyngjusandur), H55 (Hagavatn), Land1 (Landeyjarsandur), Maeli2 (Mælifellssandur), MIR45 (Myrdalssandur), which are shown in Figure 1. The coordinates of the sampling sites are reported in Table S1 in the supporting information. A comprehensive description of the sites is given in Arnalds (2010) and Arnalds et al. (2016). These extensive areas (10–140 km^2) are subjected to intensive aeolian erosion due to frequent dust storms, and significantly contribute to the total dust emissions from Iceland, which is on the order of 30–40 million tonnes per year (Arnalds et al., 2016).

In order to obtain dust particles which are representative of the particles emitted into the atmosphere, we re-suspended the surface sediment samples in atmospheric chambers and collected the PM_{10} and PM_{20} fractions (particulate matter with aerodynamic diameter < 10 µm and < 20 µm, respectively). ~~The original sediment, PM_{10} and PM_{20} were analysed for elemental and mineralogical compositions.~~

The PM_{10} samples were used for offline composition and mineralogy analyses. ~~A re-suspension apparatus was used to generate~~ PM_{10} was collected using a custom-made reactor schematically represented~~Lin sufficient quantities for the analyses. A diagram of the custom-made chamber is shown~~ in Figure S1. ~~It was composed of three main parts:~~

- ~~Injection system – Büchner flask, sieve shaker (Retsch AS200)~~
- ~~Reactor – Glass Manifold, 2 HEPA filters~~
- ~~Sampling system – PM_{10} sampling head, filter holder, vacuum pump~~

The method in Di Biagio et al. (2017) was adopted to generate dust particles, allowing for the realistic generation of dust aerosols from parent soils. ~~, was adopted for the dust particles generation.~~ Firstly, the sediment samples were sieved to < 1 mm to remove the non-erodible fraction. 15 g of sediments were placed in a Büchner flask and flushed with pure nitrogen for 10 minutes to eliminate gaseous contamination and residual water vapour. The sample was then shaken for 5 minutes at 70 Hz on a sieve shaker (Retsch AS200) and injected in ~~the reactor~~a glass manifold of approximately 1 L by nitrogen gas at 10 L min^{-1}, while the air was pumped at a flow rate of 30 L min^{-1} into a~~the~~ PM_{10} sampling head (custom-made). The PM_{10} fraction was collected on 0.4 µm polycarbonate filters and transferred into centrifuge tubes. The system was manually cleaned prior to each loading and flushed for 5 minutes with pure nitrogen to ensure an initial particle-free environment.

The PM_{20} fraction was collected using the large-scale atmospheric simulation chamber, CESAM (French acronym for Experimental Multiphasic Atmospheric Simulation Chamber)~~, a 4.2 m^3 stainless steel atmospheric simulation chamber~~ (Wang et al., 2011). The CESAM simulation facility, made of stainless steel, consists in a 4.2 m^3 multi-instrumented environmental chamber which allows to measure ~~, was used to generate the PM_{20} samples while acquiring information on~~ the size distribution and the optical properties of the generated dust aerosols while collecting filter samples for offline analysis (Di Biagio et al.,

Formatted: Normal, Space Before: 0 pt, After: 0 pt, Line spacing: single, No bullets or numbering

Formatted: Normal, Space After: 0 pt, Line spacing: single, No bullets or numbering

Formatted: Normal, Space Before: 0 pt, After: 0 pt, Line spacing: single, No bullets or numbering

Formatted: Subscript

Formatted: Superscript

2017; 2019).~~ The relation between the composition, size distribution and optical properties of the aerosol dust will be the subject of a companion paper (Baldo et al., in preparation).~~ Dust particles were generated with the sieve shaker (Retsch AS200) ~~by mechanical shaking of the sediment samples as for~~using the same protocol as for the ~~re-suspension apparatus~~small reactor as in ~~according to~~ Di Biagio et al. (2017), and injected in the CESAM chamber by flushing ~~the~~ a Büchner flask with nitrogen gas carrier at 10 L min^{-1} for 10 minutes. The dust aerosol injected in ~~the reactor~~CESAM was left suspended for about 10 minutes to allow the particle mass concentration inside the chamber to become spatially uniform. Dust particles corresponding to approximately the PM$_{20}$ fraction were extracted from the chamber using custom-made filter samplers as in Caponi et al. (2017). ~~and~~ Particles were collected by filtration on 0.4-µm pore size polycarbonate filters of 37 mm diameter at 7 L min^{-1} for approximately 1 hour. The residence time of particles in the chamber depends on their size. As shown in Di Biagio et al. (2017), particles larger than 1 µm have a lifetime of 20-30 minutes, while the lifetime of particles smaller than 1 µm can exceed a day. A second filter sample was collected successively to the first one to verify if the chemical composition of the dust was dependent on size. No significant difference was observed (not shown). The relation between the composition, size distribution and optical properties of the aerosol dust will be the subject of a companion paper (Baldo et al., in preparation).~~ Throughout the experiments, the microphysical and spectral optical properties of the suspended particles were monitored. The results will be reported in a companion paper (Baldo et al., in preparation).~~

2.2 X-ray diffraction (XRD) analysis

XRD was used to quantify the mineral phases present and to investigate the differences between the mineral fractions of dust aerosols (PM$_{10}$) and sediments. PM$_{20}$ ~~fractions~~ samples were not analysed because the ~~quantity~~ mass of dust particles collected ~~at~~ from CESAM was not sufficient for the XRD analysis. This is because the mass concentrations in the CESAM chamber is much lower compared to the custom-made reactor used for the PM$_{10}$ collection.~~.~~ The analysis was carried out at the Université de Paris, Plateforme RX UFR de Chimie, using a Panalytical Empyrean powder diffractometer equipped with a PIXcel detector fitted with a Cu anode tube (Kα1 = 1.5406 Å) operating at 45 kV and 40 mA. Diffractograms were recorded in the 5°–60° 2θ range. The samples were placed on a flat silicon monocrystalline wafer, which was loaded on the sample holder, a reflection spinner (1 s rotation time). The mineral identification was performed in Highscore Plus 3.0 (Degen et al., 2014) using the ICSD-Pan (Inorganic Crystal Structure Database) and COD (Crystallography Open Database) databases. The quantitative analysis of the mineral phases was conducted in MAUD (Material Analysis Using Diffraction). MAUD is an XRD program based on the Rietveld refinement method, which uses least square procedures to minimise the differences between the observed and calculated diffractograms (Lutterotti et al., 1999). The phase files identified with Highscore Plus were loaded as references in MAUD. It is also possible to determine the proportion of amorphous phase with the Rietveld method (Lutterotti et al., 1998). Augite was chosen as reference for the amorphous phase, having an Fe content close to MIR45, which is the samples with largest proportion of amorphous glass. The Rietveld model refines n -1 phases. As the total is fixed to100, the last phase results

Formatted: Space After: Auto

Formatted: Subscript

from the subtraction of the sum of the n refined phases. The analytical uncertainty is estimated by the software for the refined phases and represents the lower limit of the uncertainty of the proportion of each identified mineral phase.

~~The quality of the fitting was evaluated considering the χ2 calculated by the model close to one, and by comparing visually the observed and calculated diffractograms to obtain a realistic chemical model (Toby, 2006).~~The quality of the fitting was evaluated considering the χ^2 calculated by the model close to one, and by comparing visually the observed and calculated diffractograms to achieve a realistic chemical model (Toby, 2006). Small χ^2 values can be obtained when a large percentage of the intensity comes from the background (Toby, 2006). For example, the estimated χ^2 for H55 is relatively high (2.3-3.8) primarily due to missing minor mineral phases. However, H55 has the lowest fraction of amorphous material and compared to the other samples having χ^2 values very close to one, its diffraction intensities are considerably higher than the background signal.

Formatted: Not Raised by / Lowered by

Formatted: Not Raised by / Lowered by

2.3 X-ray fluorescence (XRF) analysis

PM_{10} and PM_{20} were analysed by wavelength-dispersive X-ray fluorescence (WD-XRF) to determine the elemental composition of the dust aerosols. The WD-XRF analyses were performed using a PW-2404 spectrometer by Panalytical available at LISA. Excitation X-rays are produced by a Coolidge tube (I_{max} = 125 mA, V_{max} = 60 kV) with a Rh anode. The primary X-ray spectrum is controlled by inserting filters (Al, at different thickness) between the anode and the sample. Each element was analysed three times, with specific conditions (voltage, tube filter, collimator, analysing crystal and detector), lasting 8 to 10 s.

Data were collected for 24 elements (Cl, S, Ca, Fe, Na, Mg, Al, Si, P, K, Ti, Mn, Zn, Cr, V, Ba, Co, Cu, Nd, Ni, Sr, Cd, As, Pb) using the SuperQ software. The elemental mass thickness (μg cm^{-2}), which is the analysed elemental mass per unit surface, was obtained by comparing the sample X-ray yields with those measured in the same geometry on a set of certified XRF calibration standards (Micromatter TM). ~~These standards are prepared by vacuum deposition resulting in a highly uniform deposit on a polycarbonate membrane. The standards present an element free of interferences and are thin enough to ignore thickness effects. The materials used are ≥99.9% pure and each standard thickness is certified to ±5% representing~~ Tthe ~~lower limit of the~~ uncertainty of the measured elemental concentrations ~~which~~ is around 10% (Caponi et al., 2017).

Data are reported as weight percentage of element oxides (wt%) calculated by dividing the elemental oxide mass (μg) by the total mass on filter (μg). The elemental mass on filter (μg) was first determined multiplying the measured mass thickness by the ratio between the analysed surface area and the collection area, then converted into elemental oxide mass. The total mass on filter was calculated as the sum of the mass of the oxides of the major crustal elements reported in Table 1. Fe is assumed to be as Fe_2O_3. We recognize that Fe(II) and Fe(III) can be found in the mineral phases (e.g., magnetite, augite) and in the amorphous glass, but the Fe(II)/Fe(III) ratio is not known. ~~The total Fe content (wt%) is calculated from the wt% of Fe_2O_3.~~

Formatted: Automatically adjust right indent when grid is defined, Space Before: 0 pt, Adjust space between Latin and Asian text, Adjust space between Asian text and numbers

In the XRF analysis, the concentration of light elements (atomic number Z < 19), such as Si and Al, can be underestimated due to the self-absorption of the emitted fluorescence X-Ray in the individual particles when these exceed approximately 1 µm in diameter. This is problematic when comparing elemental ratios such as Fe/Al (Formenti et al., 2010). In this study, the concentrations of light-weight elements were corrected for self-attenuation effects according to Formenti et al. (2010).

Field Code Changed

Formatted: Check spelling and grammar

2.4 Chemical weathering index

The degree of chemical weathering of Icelandic dust was calculated based on the elemental composition. This is important to evaluate the presence in the samples of secondary minerals such as clays. The chemical index of alteration (CIA) (Nesbitt and Young, 1984) was considered most suitable for the present datasets based on the chemical compositions. The CIA is interpreted as a measure of the degree of weathering of aluminium silicate minerals, (in particular feldspars) into clay minerals. In this study, the CIA was calculated according to Price and Velbel (2003) using the molecular proportion of the element oxides which were obtained by dividing the weight percentage of each oxide by the molecular weight of the oxide:~~is interpreted as a measure of the degree of weathering of aluminium silicate minerals, (in particular feldspars) into clay minerals, and it is defined as:~~

Formatted: Don't adjust right indent when grid is defined, Don't adjust space between Latin and Asian text, Don't adjust space between Asian text and numbers

$$\mathrm{CIA} = \frac{\mathrm{Al_2O_3}}{\mathrm{Al_2O_3} + \mathrm{CaO} + \mathrm{Na_2O} + \mathrm{K_2O}} \times 100$$

~~where the major element oxides are in molar fractions.~~ CIA ≤~~<~~ 50 represents the optimum fresh value, while ~~CIA >~~ 100 is the optimum weathered value. The CIA uncertainty was estimated using the error propagation formula and is ~14%.

Formatted: Don't adjust right indent when grid is defined, Space After: Auto, Don't adjust space between Latin and Asian text, Don't adjust space between Asian text and

Formatted: Space After: Auto

~~Other chemical indices were also calculated, but the CIA, the chemical index of weathering (CIW) (Harnois, 1988), and the plagioclase index of alteration (PIA) (Fedo et al., 1995) are considered most suitable for the present datasets based on the chemical compositions, each of which showed very similar results. The CIA uncertainty was calculated using the error propagation formula and is ~14%.~~

2.5 X-ray absorption near edge structure (XANES) analysis

To examine qualitatively the Fe speciation in the dust samples, XANES spectra at the Fe K-edge were collected at the Diamond Light Source beamline I18. A Si(111) double-crystal monochromator was used in the experiments. The beam size was 400x400 μm^2. The XANES spectra were collected from 7000 to 7300 eV at a resolution varying from 0.2eV for 3 sec in proximity of the Fe K-edge (7100-7125 eV) to 5eV for 1 sec from 7100-7300eV. Powder samples were suspended in methanol and deposited on kapton® tape. Filter samples were loaded without prior preparation. The analysis was repeated three times. We measured the XANES spectra of PM$_{20}$ fractions and mineral standards, including hematite and goethite standards, magnetite, feldspar standards (Clay Mineral Society), natural pyroxene and olivine. Data were processed using the Athena programme, part of the software package Demeter (ver. 0.9.26) (Ravel and Newville, 2005). For comparison, we also collected the XANES spectra for mineral dust from western Sahara and Mali (Shi et al., 2011b).

2.6 Sequential extractions

Sequential extractions of Fe were used to determine the content of Fe oxides in the PM$_{10}$ fractions. The samples were suspended in an ascorbate solution buffered at pH 7.5 to extract highly reactive amorphous Fe oxide-hydroxide (FeA) (Raiswell et al., 2008; Shi et al., 2011b; Shi et al., 2009). The ascorbate extractant was prepared by mixing a deoxygenated solution of 50 g L^{-1} sodium citrate and 50 g L^{-1} sodium bicarbonate, with 10 g L^{-1} ascorbic acid. 30 mg of dust was leached in 10 ml of ascorbate extractant continuously mixed for 24 hours. The solution was then filtered through 0.2 μm membrane filters. The residue was subsequently suspended in a dithionite solution (50 g L^{-1} sodium dithionite in 0.35 M acetic acid and 0.2 M sodium citrate) buffered at pH 4.8 for 2 hours to extract crystalline Fe oxide-hydroxide, mainly goethite and hematite (FeD).

The dithionite-oxalate sequential extraction was performed to determine the content of iron associated to magnetite (FeM) in the samples (Poulton and Canfield, 2005). First, the dust particles were treated for 2 hours with the citrate-buffered dithionite solution to remove crystalline Fe oxide-hydroxide. After filtration, the residue was leached for 6 hours in a solution of 0.2 M ammonium oxalate and 0.17 M oxalic acid at pH 3.2.

All the experiments were conducted at room temperature, in darkness. The sample solutions were continuously mixed on a rotary mixer, and then filtered through 0.2 μm membrane filters. The dissolved Fe concentration in the filtrates was measured using the ferrozine method (Viollier et al., 2000) and ICP-OES analysis for the solution containing oxalate. Each experiment was repeated 3 times. The range of relative standard deviations (rsd) for each extract for each site are: FeA, 2-18%; FeD, 1-11%; FeM, 2-15%, which have been considered as the measurement uncertainty.

2.7 Fe solubility and dissolution kinetics

The initial Fe solubility (Fe$_{isol}$) of PM$_{10}$ fractions was determined by extraction in 1.1 M ammonium acetate solution at pH 4.7 following the method in Baker et al. (2006). About 1 mg of dust was weighed on polycarbonate filters and leached for 2 hours in 10 ml of ammonium acetate solution. The solution was then filtered through 0.2 μm membrane filters and acidified to pH 2 before storage. Three replicates were performed for each sample, rsd 3-12%.

The potential Fe solubility (Fe_{psol}) was assessed through leaching experiments in sulphuric acid solution at pH2. Around 1.5 mg of dust were weighed on polycarbonate filters and leached in 50 ml of pH 2 sulphuric acid for 72 hours to simulate atmospheric acid processing similar to the method in Shi et al. (2011a, 2015). The solution was continuously stirred in darkness at room temperature. 0.5 ml of sample solution was collected at fixed time intervals (2.5 min, 15 min, 60 min, 2 hours, 6 hours, 24 hours, 48 hours and 72 hours after the dust sample was added) and filtered through 0.2 µm syringe filters into 1 ml centrifuge tubes. Dissolution kinetics of a dust sample from Africa (Libya) showed a very good repeatability with a relative standard deviation at each sampling time ranging from 4-15%.

All the experiments were conducted at room temperature, in darkness. The sample solutions were continuously mixed on a rotary mixer. The dissolved Fe concentration was measured using the ferrozine method (Viollier et al., 2000).

2.8 Volume average refractive index

The volume average refractive index ~~was~~ was calculated to evaluate the effect of the dust compositions on the optical properties ~~as in (e.g., Formenti et al., 2014b)~~. Using the volume average refractive index, we assume that the mineral phases in the dust samples are internally mixed, which ~~is~~ can be different from the real conditions and may overestimate absorption (Formenti et al., 2014b):

$$\tilde{n}(\lambda) = \sum_{j} f_j \times \tilde{n}_j(\lambda)$$

where $f_j = \frac{V_j}{V_{tot}}$ is the volume fraction of individual j minerals in the dust samples, and $\tilde{n}_j$ is the corresponding complex refractive index. The mineral volumes V_j (cm^3) are calculated as:

$$V_j = \frac{m_j}{\rho_j}$$

where $m_j = w_j \times m_{tot}$ is the mineral mass (g), w_j is the mineral mass fraction, m_{tot} is the total mass of the sample (g), and ρ_j is the mineral density (g cm^{-3}). The mineral mass fractions were obtained combining the content of the silicate minerals and glass from the XRD analysis with the contents of FeM and FeD in PM_{10}. The total mass is calculated as the sum of the element oxides mass from the XRF measurements. The densities of the crystalline phases are from webmineral.com. The density of the amorphous glass was estimated for each sample as:

$$\rho_{glass} = \frac{\rho_{dust} - \sum_j w_{jCR} \times \rho_{jCR}}{w_{glass}}$$

where ρ_{dust} is the density of the sample, ρ_{jCR} and w_{jCR} are respectively the density and the mass fraction of the crystalline phases, while w_{glass} is the mass fraction of glass. The density of the samples (fraction <63 μm) was measured by a He-pycnometer and varied from 2.80 to 3.1 g ~~/~~cm^{-3}.

Formatted: Superscript

The volume average refractive index was calculated at selected wavelength (470 nm, 520 nm, 590 nm, and 660 nm). The reference complex refractive indices of the individual minerals are reported in Table S2, when necessary the original data were interpolated at the selected wavelengths. Since it was not possible to separate the relative contribution of hematite and goethite, we assumed two extreme scenarios: FeD = goethite, FeD = hematite. For hematite, we consider two reference complex refractive from Bedidi and Cervelle (1993) and Longtin et al. (1988) as in Formenti et al. (2014b). Also for magnetite we used two different reference indices from Querry (1985) and from Huffman and Stapp (1973).

3 Results

3.1 Elemental composition

Table 1 shows the results of the XRF analysis and includes also relevant elemental ratios. The PM_{10} fractions collected using the custom-made system and PM_{20} generated using CESAM have similar elemental composition (Figure S2). The difference between PM_{10} and PM_{20} in element oxide content > 1% including CaO, Fe_2O_3, Na_2O, MgO, Al_2O_3, SiO_2 and TiO_2 is within 16%. For Fe_2O_3, Al_2O_3, SiO_2 which are the major element oxides in the dust samples, the relative differences in content are <10%. The PM_{10} and PM_{20} fractions have basaltic compositions, like the parent material, with SiO_2 representing 46-52% of the total estimated mass, and the sum of the alkali oxides (Na_2O+K_2O) between 2% and 4% (see Figure S3 in the supporting information). Al_2O_3 ranges between 11% in MIR45 to 18% in H55. H55 has the lowest Si/Al ratio (2.3-2.4), while in the other samples Si/Al is 3.1-3.7. The content of Fe_2O_3 and TiO_2 is relatively high. Fe_2O_3 is 14-16% in H55 and D3, and 17-19% in Land1, Maeli2 and MIR45. The Fe/Al ratio is from 1 to 2.2. TiO_2 is around 2-3% in H55 and D3, and 2-5.5% in Land1, Maeli2 and MIR45. CaO is 6-9% in Land1, Maeli2 and MIR45, and 10-12% in H55 and D3. The Fe/Ca ratio is 1.2-1.4 in H55 and D3, and 2.1-2.8 in Land1, Maeli2 and MIR45. Compared to D3 and H55, Land 1, Maeli2 and MIR45 have more Fe and Ti (titanium) but less Ca.

3.2 Mineralogical composition

Table 2 reports the results of the XRD analysis. The mineralogy of Icelandic dust is compatible with the parent basaltic material. The mineral composition of PM_{10} is similar to the bulk sediments. In H55, the amorphous fraction is 8% in PM_{10} and 15% in the bulk sediments. This is significantly lower than the amorphous content observed in the rest of the samples, ranging from 60 to 90%. MIR45 has the highest proportion of amorphous glass, around 90%.

Ca-rich plagioclase (anorthite) and pyroxene (augite) are the dominant mineral phases. The content of plagioclase varies respectively from around 4% in MIR45 to 46% in H55, while pyroxene is between 4% in MIR45 and 30% in H55. Olivine (forsterite) is only present in Land1 at around 7%, and in H55 1.5-1.6%. K-feldspar (microcline) is also found in Land1 and H55, but the content of K-feldspar is higher in the PM_{10} fractions, around 9% in Land1 and 10% in H55, compared to the bulk sediments 3% and 1%, respectively. XRD analysis identified (titano)magnetite in all the samples (>1%), except for D3 (see Figure S4-S8 in the supporting information).

3.3 Fe speciation

Figure 2 shows Fe phases in Icelandic dust from the sequential extractions. The total Fe (FeT) content is 10-13%, consistent with XRF analyses. The content of amorphous Fe (FeA/FeT) is 0.3-0.4% in MIR45 and H55, and around 1% in D3, Land1 and Maeli2. Dithionite Fe (FeD/FeT) is 1% in MIR45, 3-4% in D3 and H55, and about 6% in Land1 and Maeli2. Magnetite (FeM/FeT) is 7-8% in Land1 and MIR45, and around 13-15% in D3, H55 and Maeli2. About 80-90% of Fe is contained in other phases including minerals and amorphous glass.

The Fe K-edge XANES spectra of Icelandic dust have some common features (Figure 3). In the pre-edge region, there is a main peak around 7114.4 eV and a second less intense peak around 7112.7 eV. In the edge region, a main peak is observed around 7131.9 eV, but in H55 it is slightly shifted to 7131.4 eV. The presence of large quantities of amorphous material makes the quantitative analysis of the XANES spectra challenging. The presence of two peaks at 7112.7 and 7114.4 in the pre-edge region suggests that Fe is present both as Fe^{2+} and Fe^{3+} (Wilke et al., 2001). This agrees with the fact that magnetite, pyroxene and the glass phase contain Fe^{2+} and Fe^{3+}. The composition and Fe speciation of the amorphous glass varies in the different samples. H55 is the most crystalline samples (see above), and its spectral features are similar to the pyroxene standard. For all the other samples, the glass fraction is dominant, and controls their spectral characteristics.

3.4 Initial Fe solubility and dissolution kinetics

The initial Fe solubility (Fe_{isol}/FeT) is 0.08-0.2%, except in D3, which is as high as 0.6% (Figure 4). We assessed the Fe dissolution kinetic of Icelandic dust through leaching experiments in sulphuric acid at pH 2. Figure 5 shows a fast dissolution rate at the beginning, suggesting the release of Fe from highly reactive Fe phase. After 1-2 hours, the percentage of dissolved Fe increased at a slower rate, indicating that Fe solubilises from more stable phases (Shi et al., 2011a). After 72 hour-leaching, the Fe solubility in D3 and Maeli2 was 30%, up to 2 times higher than what observed for the other Icelandic dust. The potential Fe solubility after 72 hours (Fe_{psol}/FeT) is around 13% in MIR45, 17% in H55 and Land1, 26% and 29% in Maeli2 and D3, respectively.

4 Discussion

Our data indicate that Icelandic dust has basaltic composition with relatively high Fe_2O_3 and TiO_2 content (Table 1, Figure S3). The principal crystalline mineral phases observed are Ca-rich plagioclase and pyroxene, while the amorphous fraction, mostly aluminosilicate glass, is 60-90% (except for the Hagavatn hotspot, which is only 15%). Glacial processes produce fine sediments (glacial flour), which accumulates into glacial-fluvial floodplains where the dust hotspots are located (Arnalds, 2010; Arnalds et al., 2016). Our results are consistent with the composition of the volcanic systems supplying the dust hotspots: Bárðarbunga and Kverkfjöll volcanic systems (Dyngjusandur), Katla volcanic system (Mýrdalssandur, Maelifellssandur and Landeyjasandur), Eldborgir and Skersli volcanic centres (Hagavatn) (Arnalds et al., 2016; Baratoux et al., 2011; Oladottir et al., 2008).

The large amorphous fraction found in Icelandic dust and in volcanic sandy deposits is related to the volcanic activity within glaciers (Baratoux et al., 2011). The rapid cooling of magma upon the interaction with water prevents crystallisation and forms glass. Hyaloclastite deposits consisting of glass fragments are then eroded by the combined action of wind and glaciers. By contrast, sediments from the Hagavtan dust hotspots, at South of the Langjökull glacier, are from the glacial erosion of lava flows (Baratoux et al., 2011). This material is more crystalline than hyaloclastites as the rate of cooling of magma is relatively slower.

4.1 Mineralogical composition of Icelandic dust and parent sediments

Our results show that the mineralogical compositions of PM_{10} are similar to the bulk sediments from the five dust hotspots. Mineralogical fractionation is observed in African and Asian dust as a result of size segregation during emission (e.g., Claquin et al., 1999; Jeong, 2008). Quartz and K-feldspars are abundant in the soil silt fractions, while clay minerals are dominant in the clay fraction (Journet et al., 2014; Shi et al., 2005). Mineralogical fractionation is not ~~observed~~ evident in Icelandic dust, probably due to the low chemical weathering, and the lack of larger mineral grains such as quartz, K-feldspar, and clays. Only the more crystalline samples from Hagavatn showed some fractionation with respect to K-feldspar and glass, while the sediments from the other sites are derived from the glacial abrasion of hyaloclastite and thus, they tend to be more uniform.

Dagsson-Waldhauserova et al. (2015) reported the composition of dust deposited on snow after a snow-dust storm in Reykjavik. Dust was transported from the Skeidararsandur and Hagavatn hotspots. About 75% of the dust particles were volcanic glass with basaltic composition. Dagsson-Waldhauserova et al. (2014b) investigated the composition of dust from the Mælifellssandur hotspot. The dust particles were primarily composed of basaltic glass (80 wt%). The main mineral phases included plagioclases (12 wt%), pyroxenes (4.6 wt%), and olivine (2 wt%). Volcanic deposits supplying the major dust hotspots Dyngjusandur, Hagavatn, Landeyjarsandur, Mælifellssandur, and Myrdalssandur has basaltic compositions and relatively high Fe content, over 10% (Baratoux et al., 2011; Oladottir et al., 2008). Basaltic glass is the major component (up to 90%) in sediments from Dyngjusandur, Mælifellssandur, and Myrdalssandur (Baratoux et al., 2011; Moroni et al., 2018).

Baratoux et al. (2011) reported 10 wt% amorphous glass in volcanic sand from the Hagavatn hotspot area. Plagioclase, pyroxene and olivine are dominant minerals in sediments from Dyngjusandur, Hagavatn, Mælifellssandur and Myrdalssandur (Baratoux et al., 2011; Moroni et al., 2018). (Titano)magnetite has been also identified in dust and sediments (Baratoux et al., 2011; Dagsson-Waldhauserova et al., 2015; Dagsson-Waldhauserova et al., 2014b; Moroni et al., 2018; Oladottir et al., 2008) The chemical and mineralogical compositions of Icelandic dust determined in this study are comparable to those of rocks and volcanic sands from the Dyngjusandur and Hagavatn areas (Baratoux et al., 2011). The mineral phases observed in the sediments from Dyngjusandur, Mælifellssandur, and Myrdalssandur are also similar to those reported by Moroni et al. (2018).

4.2 Comparison of Icelandic dust with North African and Asian dust

In Icelandic dust the Si/Al ratio is 2.3-3.7 and the Fe/Al ratio is 1-2.2. In North African and Asian dust, Si/Al ranges between 1 and 7 (Scheuvens and Kandler, 2014). Si/Al >10 is reported in dust from the Bodele depression, which originates from Si-rich diatomite deposits (Scheuvens et al., 2013; Formenti et al., 2014b). In North African dust, Fe/Al is mainly 0.4-0.8, with similar values reported for Asian dust (Formenti et al., 2011; Scheuvens and Kandler, 2014). Compared to North African and Asian dust, Icelandic dust shows similar Si/Al, but higher Fe/Al ratio.

TiO_2 catalyses heterogeneous photochemical reactions of atmospheric trace gases including SO_2, NO_2, VOC and O_3, and contributes to the chemical balance of the atmosphere (Chen et al., 2012). In North African and Asian dust, TiO_2 is around 1% (e.g., Formenti et al., 2014b; Jeong, 2008; Shi et al., 2011b). In Icelandic dust, the element oxide concentration of Ti is relatively high 2-5.5%, although Ti can be not just as TiO_2 minerals (anatase and rutile). Ti may be present in magnetite and aluminosilicate minerals (e.g., augite) or in the amorphous glass.~~, which is significantly lower than that in Icelandic dust (2-5.5%).~~

A comparison of our results for the PM_{10} fraction to North African desert dust (Shi et al., 2011b) and Asian dust (Jeong, 2008) is provided in Figure 6. The principal minerals in Icelandic dust are Ca-rich plagioclase and pyroxene, with around 60-90% of aluminosilicate glass. The mineral composition of Icelandic dust is therefore very different from North African dust or Asian dust that derives from very different environments, which are composed mainly of quartz, feldspars, calcite and clays (Avila et al., 1997; Formenti et al., 2014b; Jeong, 2008; Jeong et al., 2016; Kandler et al., 2009; Scheuvens et al., 2013; Shao et al., 2007; Shi et al., 2011b; Shi et al., 2005).

The Fe mineralogy of Icelandic dust also differs significantly from North African and Asian dust (Figure 2). The total Fe content in Icelandic dust (10-13%) is higher than in North African dust (1-8%). In North African and Asian dust, Fe is primarily as clay minerals and Fe oxides (e.g., Formenti et al., 2014b; Shi et al., 2011b; Lafon et al., 2006; Lu et al., 2017; Takahashi et al., 2011); in particular, goethite is dominant among the crystalline Fe oxide-hydroxide (Formenti et al., 2014b; Lu et al., 2017). Icelandic dust has comparable amorphous Fe (FeA) content to North African dust, but higher magnetite and lower goethite and hematite (FeD) content. Existing observations show that the magnetite content in African dust is generally below 0.1 wt% or not detectable (Lazaro et al., 2008; Moskowitz et al., 2016). Moskowitz et al. (2016) reported 0.6 wt% magnetite in surface sediments (PM_{63}) collected in proximity of the Tibesti volcanic based on magnetic measurements. The content of magnetite reported in Asian dust source regions is in the range 0.1-0.8 wt% from magnetitic measurements and XRD analysis (Jia et al., 2019; Maher et al., 2009; Song et al., 2014). Crusius et al. (2011) reported 0.2 wt% of magnetite in glacial dust from the Copper River Valley. In Icelandic dust, the magnetite content estimated from XRD measurements and sequential extractions is 1-2 wt%.

Magnetite and to a lesser extent hematite are common in magmatic rocks (Cornell and Schwertmann, 2003). Basalts have the highest magnetite content (Cornell and Schwertmann, 2003), which explains the high magnetite content in Icelandic dust. Hematite, goethite and ferrihydrite are more likely to form during weathering (Cornell and Schwertmann, 2003). Shi et al. (2011b) observed that the content of FeA and FeD in mineral dust from North Africa was variable and dependent on the degree of weathering. The calculated CIA for Icelandic dust is below 50 (i.e., 35-45 in Table 1), indicating a low degree of weathering. The dust hotspots in Iceland are characterised by the continuous input of material by glacial-fluvial processes that prevents the alteration of minerals and the formation of soil (Arnalds, 2015).

Figure 7 shows the variation of CIA against (FeA+FeD)/FeT for both Icelandic dust and North African dust (Shi et al., 2011b). Icelandic dust is weakly weathered and has low CIA and (FeA+FeD)/FeT. By contrast, desert dust in North Africa tend to be more weathered and consequently have higher CIA and (FeA+FeD)/FeT. Having plotted the data from Shi et al. (2011b) together with the data from this study, the positive correlation between CIA and (FeA+FeD)/FeT is maintained. In summary, our results are consistent with the findings in Shi et al. (2011b) and suggest that the low content of FeA and FeD observed in the samples is related to the low degree of weathering.

The XANES Fe Kedge spectra of Icelandic dust are also quite different from those of the North African dust (Figure 3). The spectra of the two African samples (Western Sahara and Mali) have a clear double peak in the pre-edge region at around 7113.9 and 7115.2 eV, and a main peak in the edge region at around 7133.3 eV. This difference is consistent with the difference in Fe mineralogy reported above.

4.3 Factors controlling Fe solubility in Icelandic Dust

The initial fractional Fe solubility observed in mineral dust from North Africa and Asia is generally below 0.5% (Desboeufs et al., 2005; Oakes et al., 2012; Schroth et al., 2009; Shi et al., 2011c). In this study, the initial Fe solubility (Fe_{isol}/FeT) of Icelandic dust is determined through ammonium acetate extraction at pH 4.7 (Baker et al., 2006), as in Shi et al. (2011c). Icelandic dust Fe_{isol}/FeT varies from 0.08-0.6%, which is comparable to Fe_{isol}/FeT in African dust (around 0.2%) in Shi et al. (2011c) (Figure 4).

Icelandic dust has similar origin to volcanic ash. Achterberg et al. (2013) observed an initial fractional Fe solubility of 0.04-0.14% for ash from the 2011 eruption of the volcano Eyjafjallajökull (leaching in de-ionized water). Frogner et al. (2001) and Jones and Gislason (2008) reported relatively high initial fractional Fe solubility for ash from the 2000 eruption of the volcano Hekla, 2.5% for particle size 44-74 µm and 0.6% for particle size 45-125 µm (leaching in seawater). For the same volcano, Olgun et al. (2011) observed an initial fractional Fe solubility of 0.004% in the ash from the eruption in 1947 (leaching in seawater). The initial fractional Fe solubility of volcanic ash primarily depends on its surface properties determined by the eruption conditions, which can be very different from the bulk composition controlled by the source magma (Maters et al., 2017). The interaction of the ash with volcanic gases mainly HCl, SO_2 and HF within the eruption plume (plume processing) enhances the dissolution of the ash surface and the Fe mobilisation (e.g., Ayris and Delmelle, 2012; Duggen et al., 2010). As the Fe speciation on the ash surface is determined by the eruption history, the Fe dissolution behaviour can vary significantly, even for ash emitted from the same volcano (Maters et al., 2017). After deposition, the ash undergoes further processing, which contributes to modify its surface properties, consequently the Fe speciation in freshly emitted ash may be different from the Icelandic volcanic dust. The range of initial fractional Fe solubility observed for volcanic ash from Iceland is quite broad 0.004-2.5%. Although, both the volcanoes Hekla and Eyjafjallajökull have andesitic composition (e.g., Frogner et al., 2001; Olgun et al., 2011), the initial Fe solubility of Icelandic dust still lies within this range.

Icelandic dust is strongly influenced by glacial processes. The FeA and FeD content in Icelandic dust is similar to what was measured by Raiswell et al. (2016) in Ice-hosted sediments 0.03-0.2 wt% for FeA, and 0.04-0.7 wt % for FeD. Previous research investigated the initial fractional Fe solubility of dust from glacial sediments in the Copper River Valley, an important source of Fe for the Gulf of Alaska, which is Fe limited (Crusius et al., 2011; Schroth et al., 2017; Schroth et al., 2009). Glacial dust and sediments showed high initial fractional Fe solubility, which was associated to low degree of chemical weathering (Schroth et al., 2017; Schroth et al., 2009). The initial fractional Fe solubility reported for the glacial dust from the Copper River Valley is 1.4% (multiple leaches in Milli-Q water), 2-14 times higher than the initial Fe solubility observed for Icelandic dust. Mineralogy and Fe speciation control the Fe solubility in dust particles (Cwiertny et al., 2008; Fu et al., 2010; Journet et al., 2008; Schroth et al., 2009; Shi et al., 2011a). Although different methods were used, leading to uncertainties when comparing the results (Meskhidze et al., 2016), the large differences in initial fractional Fe solubility observed between the Icelandic dust and the glacial dust from the Copper River Valley here is more likely due to the distinctive mineralogy and Fe speciation. Instead, measurements conducted on snow pits from the Roosevelt Island (Antarctica), reported similar initial fractional Fe solubility to the Icelandic dust samples, around 0.7% (dissolved Fe in snow melt) (Winton et al., 2016).

Icelandic dust composition is different from North African and Asian dust, but they have similar initial Fe solubility. To better understand the factors controlling the Fe solubility in Icelandic dust we investigated the Fe dissolution kinetic at low pH. Icelandic dust showed a positive correlation between the potential Fe solubility (Fe_{psol}/FeT, defined as the fractional solubility after 72 hrs of dissolution at pH 2 sulphuric acid) and the content of pyroxene and magnetite, when the fraction of amorphous materials is significant (60-90%) (Figure S9 of the supporting information). But H55 weakens the overall correlation (Figure S9). This could be explained by the significantly higher degree of crystallinity (8-15%) observed in H55, which affects the reactivity and Fe speciation in the sample. The degree of crystallinity may directly impact the Fe solubility, as amorphous materials are generally more reactive than the crystalline forms with same composition (Wolff-Boenisch et al., 2006). However, there is no apparent correlation between the Fe_{psol} and the amorphous glass content, which was also observed for volcanic ash (Maters et al., 2017). This is because Icelandic dust consist of a mixture of crystalline minerals and glass, and the proportion of glass and its compositions vary in the different samples resulting in different solubility (Maters et al., 2017). The Fe minerals in Icelandic dust are mainly pyroxene and magnetite, and there is a minor contribution from olivine, hematite, goethite and ferrihydrite. Overall, the low degree of weathering and low crystallinity are responsible for the high potential Fe solubility in the samples.

Figure 8 shows that Icelandic dust Fe_{psol}/FeT is significantly higher than what was observed for intensively weathered desert dust such as Niger, Tibesti and Western Sahara (Shi et al., 2011b). Fe_{psol}/FeT in D3 and Maeli2 is about 30%. In H55, Land1 and MIR45, Fe_{psol}/FeT is 13-16%, which is comparable to the African samples Bodele and Tunisia. These samples are from weakly weathered paleolake sediments. Adding all the new data in this study to the data from Shi et. al (2011b) generates an inverse relationship between the degree of weathering and Fe_{psol}/FeT (Figure 8), which is consistent with the finding in Shi et al. (2011b).

4.4 Implications for the soluble Fe deposition to the ocean

The sub polar North Atlantic Ocean including the Iceland Basin is seasonally Fe-limited (Moore et al., 2006; Nielsdottir et al., 2009; Ryan-Keogh et al., 2013). Achterberg et al. (2013) reported that deposition of volcanic ash from the 2010 Eyjafjallajökull eruption caused a significant perturbation to the biogeochemistry of the Iceland Basin. Elevated dissolved Fe concentration and nitrate depletion were observed locally followed by an early spring bloom (Achterberg et al., 2013). This suggests that additional Fe inputs to the sub polar North Atlantic Ocean has the potential to perturb the biogeochemical cycling of Fe and primary production in the surface ocean.

Here we calculated the deposition of soluble Fe to the North Atlantic Ocean based on the total Fe deposition estimated in Arnalds et al. (2014), which is 0.56-1.38 Tg yr^{-1}. The initial Fe solubility of Icelandic dust reported in this study varies from 0.08-0.2% for the dust hotspots in South and Central Iceland to 0.6% for Dyngjusandur in NE Iceland. As 90% of the dust reaching the ocean is from the south coast of Iceland (Arnalds et al., 2014), a fractional Fe solubility of 0.13%, the average of the dust hotspots in South Iceland, is used in the calculation. The estimated soluble Fe deposition from Icelandic dust to the ocean is approximatively 0.73-1.79 Gg yr^{-1}. This suggests that Icelandic dust contributes to around 0.3-0.7 % of the global annual deposition flux of soluble Fe to the ocean (Myriokefalitakis et al., 2018).

4.5 Implications for the direct radiative effect

Kylling et al. (2018) estimated that in 2012 the instantaneous radiative forcing (IRF) of Icelandic dust in the Arctic was 0.02 W m^{-2} at the bottom of the atmosphere (BOA).They assumed the same optical properties for dust from different source regions, which is different from the real conditions. The mineralogical composition and the Fe speciation in Icelandic dust are different for examples from North African and Asian dust (Fig. 2, Table 2), leading to different spectral optical properties. Previous research investigated the absorption properties of volcanic sand deposited on snow, suggesting that the absorption properties of Icelandic dust from the Mýrdalssandur hotspot are similar to black carbon (Meinander et al., 2014; Peltoniemi et al., 2015). The spectral reflectance estimated for the pure volcanic sand was about 0.03, which is very similar to a black body (0.0) (Dagsson-Waldhauserova, 2014; Peltoniemi et al., 2015). Zubko et al. (2019) measured the complex refractive index of milled volcanic sand from the same area. The imaginary part of the complex refractive index (k), responsible for absorption, was 0.01 (λ = 647 nm), which is around one order of magnitude higher than the average values for natural dust from Sahel (0.002, λ = 660 nm), North Africa-Sahara and Easter Asia (0.001, λ = 660 nm) (Di Biagio et al., 2019). In the shortwave spectrum, ~~T~~the k values reported in literature for volcanic ash from Iceland range from around 0.0001 to 0.02 (Ball et al., 2015; Bukowiecki et al., 2011; Derimian et al., 2012; Hervo et al., 2012; Reed et al., 2017; Rocha-Lima et al., 2014; Schumann et al., 2011; Toledano et al., 2012; Vogel et al., 2017; Weinzierl et al., 2012), which makes it difficult to evaluate the absorption properties of volcanic dust.

Here we present a first estimate of the complex refractive index of Icelandic dust based on the mineral volume fractions determined in this study. For FeD = hematite scenario, the calculations were repeated using different reference refractive indices for hematite and magnetite, and four scenarios were considered. The real part of the volume-average refractive index ($\tilde{n}$) has an average value of 1.60 at the selected wavelengths ~~which is~~ consistently in the different scenarios. The imaginary part of the volume-average index ($\tilde{k}$) calculated using the refractive index of magnetite from Huffman and Stapp (1973) is up to one order of magnitude higher than when using the data from Querry (1985) (Table 3). No significant variations were observed applying the two different refractive indices for hematite (not shown). If using the data of magnetite from Querry (1985), $\tilde{k}$ showed little variations among the samples at the selected wavelengths, ranging from 0.001 to 0.003. While using the data from Huffman and Stapp (1973), $\tilde{k}$ generally decreased from 470 to 660 nm, and higher $\tilde{k}$ values were observed for D3, Maeli2 and H55 (0.006-0.01) compared to Land1 and MIR45 (0.004-0.006). Note that D3 has almost twice the magnetite content of Land1 and MIR45. Similar results are observed if assuming all FeD is goethite (Table 3). Overall, the estimated $\tilde{n}$ and $\tilde{k}$ are within the range reported for volcanic ash. The $\tilde{k}$ value of the dust samples from the Mýrdalssandur hotspot is 0.002-0.004 at λ = 660 nm which is 2-5 times lower than what observed in Zubko et al. (2019). The $\tilde{k}$ values estimated using the reference index of magnetite from Querry (1985) are comparable to the k values reported in Di Biagio et al. (2019) for Sahel, North Africa-Sahara and Eastern Asia. Using the magnetite refractive index from Huffman and Stapp (1973), the estimated $\tilde{k}$ values rise up to 12 times higher than the North African and Asian dust from Di Biagio et al. (2019).

Our results indicate that magnetite can be a key factor contributing to the shortwave absorption of Icelandic dust, which is in agreement with the findings in Yoshida et al. (2016), who reported the presence of strongly light absorbing mineral in Icelandic dust which were identified as magnetite-like particles. Our analysis suggests that Icelandic dust may absorb solar radiation more than North African and Asian natural dust, possibly leading to a stronger direct positive radiative effect in the Artic than the estimates by Kylling et al. (2018).

There is large uncertainty in the estimated volume-average refractive index, which is related to complex refractive index of the amorphous glass and Fe oxides (Zhang et al., 2015). In addition, the method used here may overestimate absorption as the mineral phases are considered internally mixed in the dust samples (Formenti et al., 2014b). Direct measurements are thus necessary to evaluate the optical properties of Icelandic dust, which will be reported in a separate manuscript.

5 Conclusions

In this study, we investigated the chemical composition and mineralogy of dust samples representative of five major dust hotspots in Iceland. Our results show that Icelandic dust is fundamentally different from low latitude dust. Icelandic dust has basaltic composition, and it is mainly composed of Ca-rich plagioclase, pyroxene, and amorphous glass. The amorphous materials account for 8% (Hagavatn dust hotspot) to 60-90% (Dyngjusandur, Landeyjarsandur, Mælifellssandur, Myrdalssandur hotspots) of total dust mass. Mineralogical fractionation was not observed between dust samples and sediments. Icelandic dust has high magnetite content and low hematite and goethite (FeD) and amorphous Fe (FeA). The initial Fe solubility (pH 4.7) is 0.08-0.6 %. The low degree of weathering and low crystallinity are responsible for the high Fe solubility at low pH (up to 30%).

Here we provide a comprehensive dataset including chemical composition, mineralogy, Fe speciation and Fe solubility of Icelandic dust, which can be fed to global models to estimate the flux of atmospheric soluble Fe to the sub-Arctic and Artic Oceans and to assess the radiative effect of Icelandic dust. Our analysis suggest that the shortwave absorption properties of Icelandic dust are determined by the high magnetite content, possibly leading to a stronger direct positive radiative effect in the Artic than previous estimates. The original measurements of the spectral optical properties together with the size distribution conducted at CESAM will provide further insight on the absorption properties and long range transport of Icelandic dust, necessary to estimate the radiative impact of Icelandic dust and its contribution to the Arctic warming.

Data availability. All data are reported in the manuscript.

Author contribution. CB, ZS, CDB, PF and JFD designed the experiments and discussed the results. ZS supervised the experimental and data analyses. CB performed the experiments at CESAM and the data analysis with contributions from ZS, CDB, PF, MC, EP, and JFD. The soil samples used for the experiments were collected by OA and PDV. CB and SN performed the XRD measurements. SC and PF performed the XRF measurements. CB, ZS and KI performed the XANES measurements. CB performed the Fe extractions and solubility measurements. CB and ZS prepared the manuscript with contributions from all co-authors.

Competing interests. The authors declare that they have no conflict of interest.

Acknowledgments. CB is funded by the Natural Environment Research Council (NERC) CENTA studentship (grant n.: NE/L002493/1). This paper is partly funded by the NERC highlight topic project (NE/S00579X/1). This project has received funding from the European Union’s Horizon 2020 research and innovation programme through the EUROCHAMP-2020 Infrastructure Activity under grant agreement No 730997~~This study is part of a project that has received funding from the European Union’s Horizon 2020 research and innovation programme under grant agreement No 730997~~. Part of this work was supported by the COST Action inDust (CA16202) supported by COST (European Cooperation in Science and Technology). This work was carried out with the support of the Icelandic Research Fund (Rannis) Grant No. 207057-051. We acknowledge Diamond Light Source for time on Beamline/Lab I18 under the Proposals: SP22244-1; SP12760-1; SP10327-1. The authors gratefully acknowledge Gautier Landrot (SAMBAA SOLEIL) who provided his expertise for the analysis of the XANES spectra and results. Thanks also to Giannantonio Cibin (Diamond Light Source) who provided the magnetite standard for the XANES measurements.

Formatted: Justified, Space After: Auto, Line spacing: 1.5 lines

550

6 References

Achterberg, E. P., Moore, C. M., Henson, S. A., Steigenberger, S., Stohl, A., Eckhardt, S., Avendano, L. C., Cassidy, M., Hembury, D., Klar, J. K., Lucas, M. I., Macey, A. I., Marsay, C. M., and Ryan-Keogh, T. J.: Natural iron fertilization by the Eyjafjallajökull volcanic eruption, Geophysical Research Letters, 40, 921-926, doi: 10.1002/grl.50221, 2013.

Arimoto, R.: Eolian dust and climate: relationships to sources, tropospheric chemistry, transport and deposition, Earth-Science Reviews, 54, 29-42, doi: 10.1016/s0012-8252(01)00040-x, 2001.

Arnalds, O., Gisladottir, F. O., and Sigurjonsson, H.: Sandy deserts of Iceland: an overview, Journal of Arid Environments, 47, 359-371, doi: 10.1006/jare.2000.0680, 2001.

Arnalds, O.: Dust sources and deposition of aeolian materials in Iceland, Icelandic Agricultural Sciences, 23, 3-21, 2010.

Arnalds, O., Olafsson, H., and Dagsson-Waldhauserova, P.: Quantification of iron-rich volcanogenic dust emissions and deposition over the ocean from Icelandic dust sources, Biogeosciences, 11, 6623-6632, doi: 10.5194/bg-11-6623-2014, 2014.

Arnalds, O.: The soils of Iceland, World Soils Book Series, Springer, Dordrecht, 2015.

Arnalds, O., Dagsson-Waldhauserova, P., and Olafsson, H.: The Icelandic volcanic aeolian environment: Processes and impacts — A review, Aeolian Research, 20, 176-195, doi: 10.1016/j.aeolia.2016.01.004, 2016.

Atkinson, J. D., Murray, B. J., Woodhouse, M. T., Whale, T. F., Baustian, K. J., Carslaw, K. S., Dobbie, S., O’Sullivan, D., and Malkin, T. L.: The importance of feldspar for ice nucleation by mineral dust in mixed-phase clouds, Nature, 498, 355-358, doi: 10.1038/nature12278, 2013.

Avila, A., QueraltMitjans, I., and Alarcon, M.: Mineralogical composition of African dust delivered by red rains over northeastern Spain, Journal of Geophysical Research-Atmospheres, 102, 21977-21996, doi: 10.1029/97jd00485, 1997.

Ayris, P., and Delmelle, P.: Volcanic and atmospheric controls on ash iron solubility: A review, Physics and Chemistry of the Earth, 45-46, 103-112, doi: 10.1016/j.pce.2011.04.013, 2012.

Baddock, M. C., Mockford, T., Bullard, J. E., and Thorsteinsson, T.: Pathways of high-latitude dust in the North Atlantic, Earth and Planetary Science Letters, 459, 170-182, doi: 10.1016/j.epsl.2016.11.034, 2017.

Baker, A. R., Jickells, T. D., Witt, M., and Linge, K. L.: Trends in the solubility of iron, aluminium, manganese and phosphorus in aerosol collected over the Atlantic Ocean, Marine Chemistry, 98, 43-58, doi: 10.1016/j.marchem.2005.06.004, 2006.

Ball, J. G. C., Reed, B. E., Grainger, R. G., Peters, D. M., Mather, T. A., and Pyle, D. M.: Measurements of the complex refractive index of volcanic ash at 450, 546.7, and 650nm, Journal of Geophysical Research-Atmospheres, 120, 7747-7757, doi: 10.1002/2015jd023521, 2015.

Baratoux, D., Mangold, N., Arnalds, O., Bardintzeff, J. M., Platevoët, B., Grégoire, M., and Pinet, P.: Volcanic sands of Iceland - Diverse origins of aeolian sand deposits revealed at Dyngjusandur and Lambahraun, Earth Surface Processes and Landforms, 36, 1789-1808, doi: 10.1002/esp.2201, 2011.

Bedidi, A., and Cervelle, B.: Light scattering by spherical particles with hematite and goethitelike optical properties: effect of water impregnation, Journal of Geophysical Research: Solid Earth, 98, 11941-11952, doi: 10.1029/93JB00188, 1993.

Björnsson, H., and Palsson, F.: Icelandic glaciers, Jokull, 58, 365-386, 2008.

Boucher, O., Randall, D., Artaxo, P., Bretherton, C., Feingold, G., Forster, P., Kerminen, V.-M., Kondo, Y., Liao, H., Lohmann, U., Rasch, P., Satheesh, S., Sherwood, S., Stevens, B., and Zhang, X.-Y.: Clouds and aerosols, in: Climate change 2013: the physical science basis. Contribution of Working Group I to the Fifth Assessment Report of the Intergovernmental Panel on Climate Change, edited by: Stocker, T. F., Qin, D., Plattner, G.-K., Tignor, M., Allen, S. K., Doschung, J., Nauels, A., Xia, Y., Bex, V., and Midgley, P. M., Cambridge University Press, United Kingdom and New York USA, 571-657, 2013.

Bukowiecki, N., Zieger, P., Weingartner, E., Juranyi, Z., Gysel, M., Neininger, B., Schneider, B., Hueglin, C., Ulrich, A., Wichser, A., Henne, S., Brunner, D., Kaegi, R., Schwikowski, M., Tobler, L., Wienhold, F. G., Engel, I., Buchmann, B., Peter, T., and Baltensperger, U.: Ground-based and airborne in-situ measurements of the Eyjafjallajökull volcanic aerosol plume in Switzerland in spring 2010, Atmospheric Chemistry and Physics, 11, 10011-10030, doi: 10.5194/acp-11-10011-2011, 2011.

Bullard, J. E., Baddock, M., Bradwell, T., Crusius, J., Darlington, E., Gaiero, D., Gasso, S., Gisladottir, G., Hodgkins, R., McCulloch, R., McKenna-Neuman, C., Mockford, T., Stewart, H., and Thorsteinsson, T.: High-latitude dust in the Earth system, Reviews of Geophysics, 54, 447-485, doi: 10.1002/2016rg000518, 2016.

Caponi, L., Formenti, P., Massabo, D., Di Biagio, C., Cazaunau, M., Pangui, E., Chevaillier, S., Landrot, G., Andreae, M. O., Kandler, K., Piketh, S., Saeed, T., Seibert, D., Williams, E., Balkanski, Y., Prati, P., and Doussin, J. F.: Spectral- and size-resolved mass absorption efficiency of mineral dust aerosols in the shortwave spectrum: a simulation chamber study, Atmospheric Chemistry and Physics, 17, 7175-7191, doi: 10.5194/acp-17-7175-2017, 2017.

Carslaw, K. S., Boucher, O., Spracklen, D. V., Mann, G. W., Rae, J. G. L., Woodward, S., and Kulmala, M.: A review of natural aerosol interactions and feedbacks within the Earth system, Atmospheric Chemistry and Physics, 10, 1701-1737, doi: 10.5194/acp-10-1701-2010, 2010.

Chen, H., Nanayakkara, C. E., and Grassian, V. H.: Titanium dioxide photocatalysis in atmospheric chemistry, Chemical Reviews, 112, 5919-5948, doi: 10.1021/cr3002092, 2012.

Choobari, O. A., Zawar-Reza, P., and Sturman, A.: The global distribution of mineral dust and its impacts on the climate system: A review, Atmospheric Research, 138, 152-165, doi: 10.1016/j.atmosres.2013.11.007, 2014.

Claquin, T., Schulz, M., and Balkanski, Y. J.: Modeling the mineralogy of atmospheric dust sources, Journal of Geophysical Research-Atmospheres, 104, 22243-22256, doi: 10.1029/1999jd900416, 1999.

Cornell, R. M., and Schwertmann, U.: The Iron Oxides: Structure, Properties, Reactions, Occurrence and Uses, Wiley-VCH, New York 2003.

Crusius, J., Schroth, A. W., Gasso, S., Moy, C. M., Levy, R. C., and Gatica, M.: Glacial flour dust storms in the Gulf of Alaska: Hydrologic and meteorological controls and their importance as a source of bioavailable iron, Geophysical Research Letters, 38, doi: 10.1029/2010gl046573, 2011.

Cwiertny, D. M., Baltrusaitis, J., Hunter, G. J., Laskin, A., Scherer, M. M., and Grassian, V. H.: Characterization and acid-mobilization study of iron-containing mineral dust source materials, Journal of Geophysical Research: Atmospheres, 113, doi: 10.1029/2007jd009332, 2008.

Dagsson-Waldhauserova, P.: Variability, origin and physical characteristics of dust aerosol in Iceland (PhD dissertation), Faculty of Physical Sciences Agricultural University of Iceland, Reykjavik, 163 pp., 2014.

Dagsson-Waldhauserova, P., Arnalds, O., and Olafsson, H.: Long-term variability of dust events in Iceland (1949–2011), Atmospheric Chemistry and Physics, 14, 13411-13422, doi: 10.5194/acp-14-13411-2014, 2014a.

Dagsson-Waldhauserova, P., Arnalds, O., Olafsson, H., Skrabalova, L., Sigurdardottir, G. M., Branis, M., Hladil, J., Skala, R., Navratil, T., Chadimova, L., Menar, S. V. O., Thorsteinsson, T., Carlsen, H. K., and Jonsdottir, I.: Physical properties of suspended dust during moist and low wind conditions in Iceland, Icelandic Agricultural Sciences, 27, 25-39, 2014b.

Dagsson-Waldhauserova, P., Arnalds, O., Olafsson, H., Hladil, J., Skala, R., Navratil, T., Chadimova, L., and Meinander, O.: Snow–Dust Storm: Unique case study from Iceland, March 6–7, 2013, Aeolian Research, 16, 69-74, doi: 10.1016/j.aeolia.2014.11.001, 2015.

Degen, T., Sadki, M., Bron, E., König, U., and Nénert, G.: The highscore suite, Powder Diffraction, 29, S13-S18, doi: 10.1017/S0885715614000840, 2014.

Derimian, Y., Karnieli, A., Kaufman, Y. J., Andreae, M. O., Andreae, T. W., Dubovik, O., Maenhaut, W., and Koren, I.: The role of iron and black carbon in aerosol light absorption, Atmospheric Chemistry and Physics, 8, 3623-3637, doi: 10.5194/acp-8-3623-2008, 2008.

Derimian, Y., Dubovik, O., Tanre, D., Goloub, P., Lapyonok, T., and Mortier, A.: Optical properties and radiative forcing of the Eyjafjallajökull volcanic ash layer observed over Lille, France, in 2010, Journal of Geophysical Research-Atmospheres, 117, doi: 10.1029/2011jd016815, 2012.

Desboeufs, K. V., Sofikitis, A., Losno, R., Colin, J. L., and Ausset, P.: Dissolution and solubility of trace metals from natural and anthropogenic aerosol particulate matter, Chemosphere, 58, 195-203, doi: 10.1016/j.chemosphere.2004.02.025, 2005.

Di Biagio, C., Formenti, P., Balkanski, Y., Caponi, L., Cazaunau, M., Pangui, E., Journet, E., Nowak, S., Caquineau, S., Andreae, M. O., Kandler, K., Saeed, T., Piketh, S., Seibert, D., Williams, E., and Doussin, J. F.: Global scale variability of the mineral dust long-wave refractive index: a new dataset of in situ measurements for climate modeling and remote sensing, Atmospheric Chemistry and Physics, 17, 1901-1929, doi: 10.5194/acp-17-1901-2017, 2017.

Di Biagio, C., Formenti, P., Balkanski, Y., Caponi, L., Cazaunau, M., Pangui, E., Journet, E., Nowak, S., Andreae, M. O., Kandler, K., Saeed, T., Piketh, S., Seibert, D., Williams, E., and Doussin, J. F.: Complex refractive indices and single-scattering albedo of global dust aerosols in the shortwave spectrum and relationship to size and iron content, Atmospheric Chemistry and Physics, 19, 15503-15531, doi: 10.5194/acp-19-15503-2019, 2019.

Dordevic, D., Tosic, I., Sakan, S., Petrovic, S., Duricic-Milankovic, J., Finger, D. C., and Dagsson-Waldhauserova, P.: Can Volcanic Dust Suspended From Surface Soil and Deserts of Iceland Be Transferred to Central Balkan Similarly to African Dust (Sahara)?, Frontiers in Earth Science, 7, doi: 10.3389/feart.2019.00142, 2019.

Dragosics, M., Meinander, O., Jónsdóttír, T., Dürig, T., De Leeuw, G., Pálsson, F., Dagsson-Waldhauserová, P., and Thorsteinsson, T.: Insulation effects of Icelandic dust and volcanic ash on snow and ice, Arabian Journal of Geosciences, 9, doi: 10.1007/s12517-015-2224-6, 2016.

Duggen, S., Olgun, N., Croot, P., Hoffmann, L., Dietze, H., Delmelle, P., and Teschner, C.: The role of airborne volcanic ash for the surface ocean biogeochemical iron-cycle: a review, Biogeosciences, 7, 827-844, doi: 10.5194/bg-7-827-2010, 2010.

Dumont, M., Brun, E., Picard, G., Michou, M., Libois, Q., Petit, J. R., Geyer, M., Morin, S., and Josse, B.: Contribution of light-absorbing impurities in snow to Greenland's darkening since 2009, Nature Geoscience, 7, 509-512, doi: 10.1038/ngeo2180, 2014.

Engelbrecht, J. P., Moosmuller, H., Pincock, S., Jayanty, R. K. M., Lersch, T., and Casuccio, G.: Technical note: Mineralogical, chemical, morphological, and optical interrelationships of mineral dust re-suspensions, Atmospheric Chemistry and Physics, 16, 10809-10830, doi: 10.5194/acp-16-10809-2016, 2016.

Formenti, P., Nava, S., Prati, P., Chevaillier, S., Klaver, A., Lafon, S., Mazzei, F., Calzolai, G., and Chiari, M.: Self ‐ attenuation artifacts and correction factors of light element measurements by X ‐ ray analysis: Implication for mineral dust composition studies, Journal of Geophysical Research: Atmospheres, 115, doi: 10.1029/2009JD012701, 2010.

Formenti, P., Schutz, L., Balkanski, Y., Desboeufs, K., Ebert, M., Kandler, K., Petzold, A., Scheuvens, D., Weinbruch, S., and Zhang, D.: Recent progress in understanding physical and chemical properties of African and Asian mineral dust, Atmospheric Chemistry and Physics, 11, 8231-8256, doi: 10.5194/acp-11-8231-2011, 2011.

Formenti, P., Caquineau, S., Chevaillier, S., Klaver, A., Desboeufs, K., Rajot, J. L., Belin, S., and Briois, V.: Dominance of goethite over hematite in iron oxides of mineral dust from Western Africa: Quantitative partitioning by X-ray absorption spectroscopy, Journal of Geophysical Research-Atmospheres, 119, 12740-12754, doi: 10.1002/2014jd021668, 2014a.

Formenti, P., Caquineau, S., Desboeufs, K., Klaver, A., Chevaillier, S., Journet, E., and Rajot, J. L.: Mapping the physico-chemical properties of mineral dust in western Africa: mineralogical composition, Atmospheric Chemistry and Physics, 14, 10663-10686, doi: 10.5194/acp-14-10663-2014, 2014b.

Frogner, P., Gislason, S. R., and Oskarsson, N.: Fertilizing potential of volcanic ash in ocean surface water, Geology, 29, 487-490, doi: 10.1130/0091-7613(2001)029<0487:Fpovai>2.0.Co;2, 2001.

Fu, H., Cwiertny, D. M., Carmichael, G. R., Scherer, M. M., and Grassian, V. H.: Photoreductive dissolution of Fe-containing mineral dust particles in acidic media, Journal of Geophysical Research, 115, doi: 10.1029/2009jd012702, 2010.

Groot Zwaaftink, C. D., Grythe, H., Skov, H., and Stohl, A.: Substantial contribution of northern high-latitude sources to mineral dust in the Arctic, Journal of Geophysical Research-Atmospheres, 121, 13678-13697, doi: 10.1002/2016jd025482, 2016.

Groot Zwaaftink, C. D., Arnalds, O., Dagsson-Waldhauserova, P., Eckhardt, S., Prospero, J. M., and Stohl, A.: Temporal and spatial variability of Icelandic dust emissions and atmospheric transport, Atmospheric Chemistry and Physics, 17, 10865-10878, doi: 10.5194/acp-17-10865-2017, 2017.

Haywood, J., Francis, P., Osborne, S., Glew, M., Loeb, N., Highwood, E., Tanre, D., Myhre, G., Formenti, P., and Hirst, E.: Radiative properties and direct radiative effect of Saharan dust measured by the C-130 aircraft during SHADE: 1. Solar spectrum, Journal of Geophysical Research-Atmospheres, 108, doi: 10.1029/2002jd002687, 2003.

Hervo, M., Quennehen, B., Kristiansen, N. I., Boulon, J., Stohl, A., Freville, P., Pichon, J. M., Picard, D., Labazuy, P., Gouhier, M., Roger, J. C., Colomb, A., Schwarzenboeck, A., and Sellegri, K.: Physical and optical properties of 2010 Eyjafjallajökull volcanic eruption aerosol: ground-based, Lidar and airborne measurements in France, Atmospheric Chemistry and Physics, 12, 1721-1736, doi: 10.5194/acp-12-1721-2012, 2012.

Huffman, D. R., and Stapp, J. L.: Optical measurements on solids of possible interstellar importance, in: Interstellar dust and related topics, Springer, 297-301, 1973.

Jakobsson, S. P., and Gudmundsson, M. T.: Subglacial and intraglacial volcanic formations in Iceland, Jokull, 58, 179-196, 2008.

Jensen, E. H., Egilson, D., Pagneux, E., Björnsson, B. B., Zóphóníasson, S., Snorrason, S. P., Jónsdóttir, I., Þrastarson, R. H., igurðsson, O. S., and Roberts, M. J.: Hættumat vegna jökulhlaupa í Skaftá [Danger of Skafta jokulhlaup]. Icelandic

Meteorological Office Report VÍ 2018-0xx, available at http://www.vedur.is/media/Eplican%C3%A1mskei%C3%B0/2018_skaftarhlaup_soguleg_gogn_lokadrog_rs.pdf (last access: 04 January 2020), 2018.

Jeong, G. Y.: Bulk and single-particle mineralogy of Asian dust and a comparison with its source soils, Journal of Geophysical Research-Atmospheres, 113, doi: 10.1029/2007jd008606, 2008.

Jeong, G. Y., Park, M. Y., Kandler, K., Nousiainen, T., and Kemppinen, O.: Mineralogical properties and internal structures of individual fine particles of Saharan dust, Atmospheric Chemistry and Physics, 16, 12397-12410, doi: 10.5194/acp-16-12397-2016, 2016.

Jia, J., Wang, Y. J., Xia, D. S., Lu, H., and Gao, F. Y.: Dust Sources of Last Glacial Chinese Loess Based on the Iron Mineralogy of Fractionated Source Samples, Geophysical Research Letters, 46, 2103-2110, doi: 10.1029/2018gl080909, 2019.

Jickells, T., and Moore, C. M.: The importance of Atmospheric Deposition for Ocean Productivity, Annual Review of Ecology, Evolution, and Systematics, 46, 481-501, doi: 10.1146/annurev-ecolsys-120213-054118, 2015.

Jickells, T. D., An, Z. S., Andersen, K. K., Baker, A. R., Bergametti, G., Brooks, N., Cao, J. J., Boyd, P. W., Duce, R. A., Hunter, K. A., Kawahata, H., Kubilay, N., laRoche, J., Liss, P. S., Mahowald, N., Prospero, J. M., Ridgwell, A. J., Tegen, I., and Torres, R.: Global iron connections between desert dust, ocean biogeochemistry, and climate, Science, 308, 67-71, doi: 10.1126/science.1105959, 2005.

Jones, M. T., and Gislason, S. R.: Rapid releases of metal salts and nutrients following the deposition of volcanic ash into aqueous environments, Geochimica Et Cosmochimica Acta, 72, 3661-3680, doi: 10.1016/j.gca.2008.05.030, 2008.

Journet, E., Desboeufs, K. V., Caquineau, S., and Colin, J. L.: Mineralogy as a critical factor of dust iron solubility, Geophysical Research Letters, 35, doi: 10.1029/2007gl031589, 2008.

Journet, E., Balkanski, Y., and Harrison, S. P.: A new data set of soil mineralogy for dust-cycle modeling, Atmospheric Chemistry and Physics, 14, 3801-3816, doi: 10.5194/acp-14-3801-2014, 2014.

Kanakidou, M., Myriokefalitakis, S., and Tsigaridis, K.: Aerosols in atmospheric chemistry and biogeochemical cycles of nutrients, Environmental Research Letters, 13, doi: 10.1088/1748-9326/aabcdb, 2018.

Kandler, K., Schutz, L., Deutscher, C., Ebert, M., Hofmann, H., Jackel, S., Jaenicke, R., Knippertz, P., Lieke, K., Massling, A., Petzold, A., Schladitz, A., Weinzierl, B., Wiedensohler, A., Zorn, S., and Weinbruch, S.: Size distribution, mass concentration, chemical and mineralogical composition and derived optical parameters of the boundary layer aerosol at Tinfou, Morocco, during SAMUM 2006, Tellus Series B-Chemical and Physical Meteorology, 61, 32-50, doi: 10.1111/j.1600-0889.2008.00385.x, 2009.

Kylling, A., Zwaaftink, C. D. G., and Stohl, A.: Mineral Dust Instantaneous Radiative Forcing in the Arctic, Geophysical Research Letters, 45, 4290-4298, doi: 10.1029/2018gl077346, 2018.

Lafon, S., Sokolik, I. N., Rajot, J. L., Caquineau, S., and Gaudichet, A.: Characterization of iron oxides in mineral dust aerosols: Implications for light absorption, Journal of Geophysical Research-Atmospheres, 111, doi: 10.1029/2005jd007016, 2006.

Lazaro, F. J., Gutierrez, L., Barron, V., and Gelado, M. D.: The speciation of iron in desert dust collected in Gran Canaria (Canary Islands): Combined chemical, magnetic and optical analysis, Atmospheric Environment, 42, 8987-8996, doi: 10.1016/j.atmosenv.2008.09.035, 2008.

Longtin, D. R., Shettle, E. P., Hummel, J. R., and Pryce, J. D.: A wind dependent desert aerosol model: Radiative properties, AFGLTR-88-0112, Air Force Geophysics Laboratory, Hanscom AFB, MA, 1988.

Lu, W. Y., Zhao, W. C., Balsam, W., Lu, H., Liu, P., Lu, Z. L., and Ji, J. F.: Iron Mineralogy and Speciation in Clay-Sized Fractions of Chinese Desert Sediments, Journal of Geophysical Research-Atmospheres, 122, 13458-13471, doi: 10.1002/2017jd027733, 2017.

Lutterotti, L., Ceccato, R., Dal Maschio, R., and Pagani, E.: Quantitative analysis of silicate glass in ceramic materials by the Rietveld method, Materials Science Forum, 278, 87-92, 1998.

Lutterotti, L., Matthies, S., and Wenk, H.: MAUD: a friendly Java program for material analysis using diffraction, IUCr: Newsletter of the CPD, 21, 1999.

Maher, B. A., Mutch, T. J., and Cunningham, D.: Magnetic and geochemical characteristics of Gobi Desert surface sediments: Implications for provenance of the Chinese Loess Plateau, Geology, 37, 279-282, doi: 10.1130/g25293a.1, 2009.

Maher, B. A., Prospero, J. M., Mackie, D., Gaiero, D., Hesse, P. P., and Balkanski, Y.: Global connections between aeolian dust, climate and ocean biogeochemistry at the present day and at the last glacial maximum, Earth-Science Reviews, 99, 61-97, doi: 10.1016/j.earscirev.2009.12.001, 2010.

Mahowald, N. M., Kloster, S., Engelstaedter, S., Moore, J. K., Mukhopadhyay, S., McConnell, J. R., Albani, S., Doney, S. C., Bhattacharya, A., Curran, M. A. J., Flanner, M. G., Hoffman, F. M., Lawrence, D. M., Lindsay, K., Mayewski, P. A., Neff, J., Rothenberg, D., Thomas, E., Thornton, P. E., and Zender, C. S.: Observed 20th century desert dust variability: impact on climate and biogeochemistry, Atmospheric Chemistry and Physics, 10, 10875-10893, doi: 10.5194/acp-10-10875-2010, 2010.

Maters, E. C., Delmelle, P., and Gunnlaugsson, H. P.: Controls on iron mobilisation from volcanic ash at low pH: Insights from dissolution experiments and Mossbauer spectroscopy, Chemical Geology, 449, 73-81, doi: 10.1016/j.chemgeo.2016.11.036, 2017.

Meinander, O., Kontu, A., Virkkula, A., Arola, A., Backman, L., Dagsson-Waldhauserová, P., Järvinen, O., Manninen, T., Svensson, J., de Leeuw, G., and Leppäranta, M.: Brief communication: Light-absorbing impurities can reduce the density of melting snow, The Cryosphere, 8, 991-995, doi: 10.5194/tc-8-991-2014, 2014.

Meskhidze, N., Johnson, M. S., Hurley, D., and Dawson, K.: Influence of measurement uncertainties on fractional solubility of iron in mineral aerosols over the oceans, Aeolian Research, 22, 85-92, doi: 10.1016/j.aeolia.2016.07.002, 2016.

Möller, R., Möller, M., Kukla, P. A., and Schneider, C.: Impact of supraglacial deposits of tephra from Grímsvötn volcano, Iceland, on glacier ablation, Journal of Glaciology, 62, 933-943, doi: 10.1017/jog.2016.82, 2016.

Möller, R., Möller, M., Kukla, P. A., and Schneider, C.: Modulation of glacier ablation by tephra coverage from Eyjafjallajökull and Grimsvötn volcanoes, Iceland: an automated field experiment, Earth System Science Data, 10, 53-60, doi: 10.5194/essd-10-53-2018, 2018.

Moore, C. M., Mills, M. M., Milne, A., Langlois, R., Achterberg, E. P., Lochte, K., Geider, R. J., and La Roche, J.: Iron limits primary productivity during spring bloom development in the central North Atlantic, Global Change Biology, 12, 626-634, doi: 10.1111/j.1365-2486.2006.01122.x, 2006.

Moosmuller, H., Engelbrecht, J. P., Skiba, M., Frey, G., Chakrabarty, R. K., and Arnott, W. P.: Single scattering albedo of fine mineral dust aerosols controlled by iron concentration, Journal of Geophysical Research-Atmospheres, 117, doi: 10.1029/2011jd016909, 2012.

Moroni, B., Arnalds, O., Dagsson-Waldhauserova, P., Crocchianti, S., Vivani, R., and Cappelletti, D.: Mineralogical and Chemical Records of Icelandic Dust Sources Upon Ny-angstrom lesund (Svalbard Islands), Frontiers in Earth Science, 6, doi: 10.3389/feart.2018.00187, 2018.

Moskowitz, B. M., Reynolds, R. L., Goldstein, H. L., Berquo, T. S., Kokaly, R. F., and Bristow, C. S.: Iron oxide minerals in dust-source sediments from the Bodele Depression, Chad: Implications for radiative properties and Fe bioavailability of dust plumes from the Sahara, Aeolian Research, 22, 93-106, doi: 10.1016/j.aeolia.2016.07.001, 2016.

Myriokefalitakis, S., Ito, A., Kanakidou, M., Nenes, A., Krol, M. C., Mahowald, N. M., Scanza, R. A., Hamilton, D. S., Johnson, M. S., Meskhidze, N., Kok, J. F., Guieu, C., Baker, A. R., Jickells, T. D., Sarin, M. M., Bikkina, S., Shelley, R., Bowie, A., Perron, M. M. G., and Duce, R. A.: Reviews and syntheses: the GESAMP atmospheric iron deposition model intercomparison study, Biogeosciences, 15, 6659-6684, doi: 10.5194/bg-15-6659-2018, 2018.

Nesbitt, H. W., and Young, G. M.: Prediction of some weathering trends of plutonic and volcanic-rocks based on thermodynamic and kinetic considerations, Geochimica Et Cosmochimica Acta, 48, 1523-1534, doi: 10.1016/0016-7037(84)90408-3, 1984.

Nielsdottir, M. C., Moore, C. M., Sanders, R., Hinz, D. J., and Achterberg, E. P.: Iron limitation of the postbloom phytoplankton communities in the Iceland Basin, Global Biogeochemical Cycles, 23, doi: 10.1029/2008gb003410, 2009.

Oakes, M., Ingall, E. D., Lai, B., Shafer, M. M., Hays, M. D., Liu, Z. G., Russell, A. G., and Weber, R. J.: Iron Solubility Related to Particle Sulfur Content in Source Emission and Ambient Fine Particles, Environmental Science & Technology, 46, 6637-6644, doi: 10.1021/es300701c, 2012.

Oladottir, B. A., Sigmarsson, O., Larsen, G., and Thordarson, T.: Katla volcano, Iceland: magma composition, dynamics and eruption frequency as recorded by Holocene tephra layers, Bulletin of Volcanology, 70, 475-493, doi: 10.1007/s00445-007-0150-5, 2008.

Olgun, N., Duggen, S., Croot, P. L., Delmelle, P., Dietze, H., Schacht, U., Oskarsson, N., Siebe, C., Auer, A., and Garbe-Schonberg, D.: Surface ocean iron fertilization: The role of airborne volcanic ash from subduction zone and hot spot volcanoes and related iron fluxes into the Pacific Ocean, Global Biogeochemical Cycles, 25, doi: 10.1029/2009gb003761, 2011.

Oskarsson, N.: The interaction between volcanic gases and tephra - fluorine adhering to tephra of the 1970 Hekla eruption, Journal of Volcanology and Geothermal Research, 8, 251-266, doi: 10.1016/0377-0273(80)90107-9, 1980.

Paramonov, M., David, R. O., Kretzschmar, R., and Kanji, Z. A.: A laboratory investigation of the ice nucleation efficiency of three types of mineral and soil dust, Atmospheric Chemistry and Physics, 18, 16515-16536, doi: 10.5194/acp-18-16515-2018, 2018.

Peltoniemi, J. I., Gritsevich, M., Hakala, T., Dagsson-Waldhauserova, P., Arnalds, O., Anttila, K., Hannula, H. R., Kivekas, N., Lihavainen, H., Meinander, O., Svensson, J., Virkkula, A., and de Leeuw, G.: Soot on Snow experiment: bidirectional reflectance factor measurements of contaminated snow, Cryosphere, 9, 2323-2337, doi: 10.5194/tc-9-2323-2015, 2015.

Poulton, S. W., and Canfield, D. E.: Development of a sequential extraction procedure for iron: implications for iron partitioning in continentally derived particulates, Chemical Geology, 214, 209-221, doi: 10.1016/j.chemgeo.2004.09.003, 2005.

Price, J. R., and Velbel, M. A.: Chemical weathering indices applied to weathering profiles developed on heterogeneous felsic metamorphic parent rocks, Chemical Geology, 202, 397-416, doi: 10.1016/j.chemgeo.2002.11.001, 2003.

Prospero, J. M., Bullard, J. E., and Hodgkins, R.: High-Latitude Dust Over the North Atlantic: Inputs from Icelandic Proglacial Dust Storms, Science, 335, 1078-1082, doi: 10.1126/science.1217447, 2012.

Qian, Y., Yasunari, T. J., Doherty, S. J., Flanner, M. G., Lau, W. K. M., Ming, J., Wang, H. L., Wang, M., Warren, S. G., and Zhang, R. D.: Light-absorbing Particles in Snow and Ice: Measurement and Modeling of Climatic and Hydrological impact, Advances in Atmospheric Sciences, 32, 64-91, doi: 10.1007/s00376-014-0010-0, 2015.

Querry, M. R.: Magnetite, Refractive index database, available at https://refractiveindex.info/?shelf=main&book=Fe3O4& (last access: 02 January 2020), 1985.

Raiswell, R., Benning, L. G., Tranter, M., and Tulaczyk, S.: Bioavailable iron in the Southern Ocean: the significance of the iceberg conveyor belt, Geochemical Transactions, 9, doi: 10.1186/1467-4866-9-7, 2008.

Raiswell, R., Hawkings, J. R., Benning, L. G., Baker, A. R., Death, R., Albani, S., Mahowald, N., Krom, M. D., Poulton, S. W., and Wadham, J.: Potentially bioavailable iron delivery by iceberg-hosted sediments and atmospheric dust to the polar oceans, Biogeosciences, 13, 3887-3900, doi: 10.5194/bg-13-3887-2016, 2016.

Ravel, B., and Newville, M.: ATHENA, ARTEMIS, HEPHAESTUS: data analysis for X-ray absorption spectroscopy using IFEFFIT, Journal of synchrotron radiation, 12, 537-541, doi: 10.1107/S0909049505012719, 2005.

Reed, B. E., Peters, D. M., McPheat, R., Smith, A. J. A., and Grainger, R. G.: Mass extinction spectra and size distribution measurements of quartz and amorphous silica aerosol at 0.33-19 mu m compared to modelled extinction using Mie, CDE, and T-matrix theories, Journal of Quantitative Spectroscopy & Radiative Transfer, 199, 52-65, doi: 10.1016/j.jqsrt.2017.05.011, 2017.

Rocha-Lima, A., Martins, J. V., Remer, L. A., Krotkov, N. A., Tabacniks, M. H., Ben-Ami, Y., and Artaxo, P.: Optical, microphysical and compositional properties of the Eyjafjallajökull volcanic ash, Atmospheric Chemistry and Physics, 14, 10649-10661, doi: 10.5194/acp-14-10649-2014, 2014.

Ryan-Keogh, T. J., Macey, A. I., Nielsdottir, M. C., Lucas, M. I., Steigenberger, S. S., Stinchcombe, M. C., Achterberg, E. P., Bibby, T. S., and Moore, C. M.: Spatial and temporal development of phytoplankton iron stress in relation to bloom dynamics in the high-latitude North Atlantic Ocean, Limnology and Oceanography, 58, 533-545, doi: 10.4319/lo.2013.58.2.0533, 2013.

Scheuvens, D., Schutz, L., Kandler, K., Ebert, M., and Weinbruch, S.: Bulk composition of northern African dust and its source sediments - A compilation, Earth-Science Reviews, 116, 170-194, doi: 10.1016/j.earscirev.2012.08.005, 2013.

Scheuvens, D., and Kandler, K.: On composition, morphology, and size distribution of airborne mineral dust, in: Mineral Dust, Springer, 15-49, 2014.

Schroth, A. W., Crusius, J., Sholkovitz, E. R., and Bostick, B. C.: Iron solubility driven by speciation in dust sources to the ocean, Nature Geoscience, 2, 337-340, doi: 10.1038/ngeo501, 2009.

Schroth, A. W., Crusius, J., Gasso, S., Moy, C. M., Buck, N. J., Resing, J. A., and Campbell, R. W.: Atmospheric deposition of glacial iron in the Gulf of Alaska impacted by the position of the Aleutian Low, Geophysical Research Letters, 44, 5053-5061, doi: 10.1002/2017gl073565, 2017.

Schumann, U., Weinzierl, B., Reitebuch, O., Schlager, H., Minikin, A., Forster, C., Baumann, R., Sailer, T., Graf, K., Mannstein, H., Voigt, C., Rahm, S., Simmet, R., Scheibe, M., Lichtenstern, M., Stock, P., Ruba, H., Schauble, D., Tafferner, A., Rautenhaus, M., Gerz, T., Ziereis, H., Krautstrunk, M., Mallaun, C., Gayet, J. F., Lieke, K., Kandler, K., Ebert, M., Weinbruch, S., Stohl, A., Gasteiger, J., Gross, S., Freudenthaler, V., Wiegner, M., Ansmann, A., Tesche, M., Olafsson, H., and Sturm, K.: Airborne observations of the Eyjafjalla volcano ash cloud over Europe during air space closure in April and May 2010, Atmospheric Chemistry and Physics, 11, 2245-2279, doi: 10.5194/acp-11-2245-2011, 2011.

Shao, L. Y., Li, W. J., Yang, S. S., Shi, Z., and Lu, S. L.: Mineralogical characteristics of airborne particles collected in Beijing during a severe Asian dust storm period in spring 2002, Science in China Series D-Earth Sciences, 50, 953-959, doi: 10.1007/s11430-007-0035-7, 2007.

Shi, Z., Shao, L. T., Jones, T. P., and Lu, S. L.: Microscopy and mineralogy of airborne particles collected during severe dust storm episodes in Beijing, China, Journal of Geophysical Research-Atmospheres, 110, doi: 10.1029/2004jd005073, 2005.

Shi, Z., Krom, M. D., Bonneville, S., Baker, A. R., Jickells, T. D., and Benning, L. G.: Formation of iron nanoparticles and increase in iron reactivity in the mineral dust during simulated cloud processing, Environmental Science & Technology, 43, 6592-6596, doi: 10.1021/es901294g, 2009.

Shi, Z., Bonneville, S., Krom, M. D., Carslaw, K. S., Jickells, T. D., Baker, A. R., and Benning, L. G.: Iron dissolution kinetics of mineral dust at low pH during simulated atmospheric processing, Atmospheric Chemistry and Physics, 11, 995-1007, doi: 10.5194/acp-11-995-2011, 2011a.

Shi, Z., Krom, M. D., Bonneville, S., Baker, A. R., Bristow, C., Drake, N., Mann, G., Carslaw, K., McQuaid, J. B., Jickells, T., and Benning, L. G.: Influence of chemical weathering and aging of iron oxides on the potential iron solubility of Saharan dust during simulated atmospheric processing, Global Biogeochemical Cycles, 25, doi: 10.1029/2010gb003837, 2011b.

Shi, Z., Woodhouse, M. T., Carslaw, K. S., Krom, M. D., Mann, G. W., Baker, A. R., Savov, I., Fones, G. R., Brooks, B., Drake, N., Jickells, T. D., and Benning, L. G.: Minor effect of physical size sorting on iron solubility of transported mineral dust, Atmospheric Chemistry and Physics, 11, 8459-8469, doi: 10.5194/acp-11-8459-2011, 2011c.

Shi, Z., Krom, M. D., Jickells, T. D., Bonneville, S., Carslaw, K. S., Mihalopoulos, N., Baker, A. R., and Benning, L. G.: Impacts on iron solubility in the mineral dust by processes in the source region and the atmosphere: A review, Aeolian Research, 5, 21-42, doi: 10.1016/j.aeolia.2012.03.001, 2012.

Shi, Z., Krom, M. D., Bonneville, S., and Benning, L. G.: Atmospheric processing outside clouds increases soluble iron in mineral dust, Environmental Science & Technology, 49, 1472-1477, doi: 10.1021/es504623x, 2015.

Sokolik, I. N., and Toon, O. B.: Incorporation of mineralogical composition into models of the radiative properties of mineral aerosol from UV to IR wavelengths, Journal of Geophysical Research-Atmospheres, 104, 9423-9444, doi: 10.1029/1998jd200048, 1999.

Song, Y. G., Chen, X. L., Qian, L. B., Li, C. X., Li, Y., Li, X. X., Chang, H., and An, Z. S.: Distribution and composition of loess sediments in the Ili Basin, Central Asia, Quaternary International, 334, 61-73, doi: 10.1016/j.quaint.2013.12.053, 2014.

Stockdale, A., Krom, M. D., Mortimer, R. J., Benning, L. G., Carslaw, K. S., Herbert, R. J., Shi, Z., Myriokefalitakis, S., Kanakidou, M., and Nenes, A.: Understanding the nature of atmospheric acid processing of mineral dusts in supplying bioavailable phosphorus to the oceans, Proceedings of the National Academy of Sciences of the United States of America, 113, 14639-14644, doi: 10.1073/pnas.1608136113, 2016.

Takahashi, Y., Higashi, M., Furukawa, T., and Mitsunobu, S.: Change of iron species and iron solubility in Asian dust during the long-range transport from western China to Japan, Atmospheric Chemistry and Physics, 11, 11237-11252, doi: 10.5194/acp-11-11237-2011, 2011.

Tang, M. J., Cziczo, D. J., and Grassian, V. H.: Interactions of Water with Mineral Dust Aerosol: Water Adsorption, Hygroscopicity, Cloud Condensation, and Ice Nucleation, Chemical Reviews, 116, 4205-4259, doi: 10.1021/acs.chemrev.5b00529, 2016.

Toby, B. H.: R factors in Rietveld analysis: How good is good enough?, Powder diffraction, 21, 67-70, doi: 10.1154/1.2179804, 2006.

Toledano, C., Bennouna, Y., Cachorro, V., de Galisteo, J. P. O., Stohl, A., Stebel, K., Kristiansen, N. I., Olmo, F. J., Lyamani, H., Obregon, M. A., Estelles, V., Wagner, F., Baldasano, J. M., Gonzalez-Castanedo, Y., Clarisse, L., and de Frutos, A. M.: Aerosol properties of the Eyjafjallajökull ash derived from sun photometer and satellite observations over the Iberian Peninsula, Atmospheric Environment, 48, 22-32, doi: 10.1016/j.atmosenv.2011.09.072, 2012.

Urupina, D., Lasne, J., Romanias, M. N., Thiery, V., Dagsson-Waldhauserova, P., and Thevenet, F.: Uptake and surface chemistry of SO2 on natural volcanic dusts, Atmospheric Environment, 217, doi: 10.1016/j.atmosenv.2019.116942, 2019.

Vergara-Temprado, J., Miltenberger, A. K., Furtado, K., Grosvenor, D. P., Shipway, B. J., Hill, A. A., Wilkinson, J. M., Field, P. R., Murray, B. J., and Carslaw, K. S.: Strong control of Southern Ocean cloud reflectivity by ice-nucleating particles, Proceedings of the National Academy of Sciences, 115, 2687-2692, doi: 10.1073/pnas.1721627115, 2018.

Viollier, E., Inglett, P. W., Hunter, K., Roychoudhury, A. N., and Van Cappellen, P.: The ferrozine method revisited: Fe(II)/Fe(III) determination in natural waters, Applied Geochemistry, 15, 785-790, doi: 10.1016/s0883-2927(99)00097-9, 2000.

Vogel, A., Diplas, S., Durant, A. J., Azar, A. S., Sunding, M. F., Rose, W. I., Sytchkova, A., Bonadonna, C., Kruger, K., and Stohl, A.: Reference data set of volcanic ash physicochemical and optical properties, Journal of Geophysical Research-Atmospheres, 122, 9485-9514, doi: 10.1002/2016jd026328, 2017.

Wang, J., Doussin, J. F., Perrier, S., Perraudin, E., Katrib, Y., Pangui, E., and Picquet-Varrault, B.: Design of a new multi-phase experimental simulation chamber for atmospheric photosmog, aerosol and cloud chemistry research, Atmospheric Measurement Techniques, 4, 2465-2494, doi: 10.5194/amt-4-2465-2011, 2011.

Weinzierl, B., Sauer, D., Minikin, A., Reitebuch, O., Dahlkotter, F., Mayer, B., Emde, C., Tegen, I., Gasteiger, J., Petzold, A., Veira, A., Kueppers, U., and Schumann, U.: On the visibility of airborne volcanic ash and mineral dust from the pilot's perspective in flight, Physics and Chemistry of the Earth, 45-46, 87-102, doi: 10.1016/j.pce.2012.04.003, 2012.

Wilke, M., Farges, F., Petit, P. E., Brown, G. E., and Martin, F.: Oxidation state and coordination of Fe in minerals: An FeK-XANES spectroscopic study, American Mineralogist, 86, 714-730, doi: 10.2138/am-2001-5-612, 2001.

Winton, V. H. L., Edwards, R., Delmonte, B., Ellis, A., Andersson, P. S., Bowie, A., Bertler, N. A. N., Neff, P., and Tuohy, A.: Multiple sources of soluble atmospheric iron to Antarctic waters, Global Biogeochemical Cycles, 30, 421-437, doi: 10.1002/2015gb005265, 2016.

Wittmann, M., Zwaaftink, C. D. G., Schmidt, L. S., Gudmundsson, S., Palsson, F., Arnalds, O., Björnsson, H., Thorsteinsson, T., and Stohl, A.: Impact of dust deposition on the albedo of Vatnajökull ice cap, Iceland, Cryosphere, 11, 741-754, doi: 10.5194/tc-11-741-2017, 2017.

Wolff-Boenisch, D., Gislason, S. R., and Oelkers, E. H.: The effect of crystallinity on dissolution rates and CO2 consumption capacity of silicates, Geochimica Et Cosmochimica Acta, 70, 858-870, doi: 10.1016/j.gca.2005.10.016, 2006.

Yoshida, A., Moteki, N., Ohata, S., Mori, T., Tada, R., Dagsson-Waldhauserová, P., and Kondo, Y.: Detection of light-absorbing iron oxide particles using a modified single-particle soot photometer, Aerosol Science and Technology, 50, 1-4, doi: 10.1080/02786826.2016.1146402, 2016.

Zhang, X. L., Wu, G. J., Zhang, C. L., Xu, T. L., and Zhou, Q. Q.: What is the real role of iron oxides in the optical properties of dust aerosols?, Atmospheric Chemistry and Physics, 15, 12159-12177, doi: 10.5194/acp-15-12159-2015, 2015.

Zubko, N., Munoz, O., Zubko, E., Gritsevich, M., Escobar-Cerezo, J., Berg, M. J., and Peltoniemi, J.: Light scattering from volcanic-sand particles in deposited and aerosol form, Atmospheric Environment, 215, doi: 10.1016/j.atmosenv.2019.06.051, 2019.

Table 1: Elemental oxide mass percentages, chemical index of alteration (CIA), and relevant elemental ratios in PM$_{10}$ (custom-made reactor) and PM$_{20}$ (CESAM chamber).

Sample	Size fraction	Element oxide mass wt%										CIA	Si/Al	Fe/Al	Ca/Fe
		CaO	Fe_2O_3	Na_2O	MgO	Al_2O_3	SiO_2	P_2O_5	K_2O	TiO_2	MnO				
D3	PM$_{10}$	11.6	16.3	2.3	4.9	13.7	47.5	0.2	0.5	2.7	0.3	35	3.06	1.58	1.38
H55	PM$_{10}$	12.4	15.1	1.9	5.1	16.9	46.0	0.1	0.2	2.2	0.2	39	2.41	1.19	1.19
Land1	PM$_{10}$	6.9	18.2	2.5	2.4	12.7	50.8	0.4	1.4	4.3	0.3	41	3.52	1.88	2.56
Maeli2	PM$_{10}$	8.5	18.4	2.4	3.9	12.7	47.7	0.3	0.9	4.9	0.3	38	3.31	1.92	2.13
MIR45	PM$_{10}$	8.6	18.8	2.6	4.0	11.4	47.4	0.4	0.9	5.5	0.4	35	3.68	2.18	2.14
D3	PM$_{20}$	10.3	14.8	2.3	5.0	13.7	50.7	0.2	0.4	2.4	0.2	37	3.26	1.42	1.41
H55	PM$_{20}$	11.3	13.8	2.2	5.1	18.1	47.1	0.1	0.1	2.0	0.2	43	2.30	1.01	1.20
Land1	PM$_{20}$	5.8	16.8	2.9	2.8	13.6	52.2	0.5	1.2	4.0	0.3	45	3.39	1.63	2.82
Maeli2	PM$_{20}$	7.6	17.6	2.5	3.9	13.1	49.2	0.3	0.8	4.7	0.2	41	3.32	1.78	2.26
MIR45	PM$_{20}$	8.3	18.8	2.8	4.0	11.7	47.9	0.4	0.9	5.0	0.3	36	3.61	2.11	2.22

Note: The data uncertainty was estimated using the error propagation formula: ~12% for the elemental oxide mass percentage, ~14% for CIA and the element ratios.

Table 2: Mineralogical composition of PM$_{10}$ and sediments. Standard deviation (sd) of the identified mineral phases are estimated by the MAUD software, except for anorthite which is calculated using the error propagation formula.

Samples	Size fraction	Anorthite wt% (sd)	Augite wt% (sd)	Forsterite wt% (sd)	Microcline wt% (sd)	Quartz wt% (sd)	Ti-Magnetite wt% (sd)	Glass wt% (sd)	χ^2
D3	PM$_{10}$	14.9 (0.9)	13.4 (0.2)	-	-	-	-	71.7 (0.9)	1.0
H55	PM$_{10}$	43.3 (1.7)	29.7 (0.4)	7.3 (0.3)	10.3 (0.6)	-	1.3 (0.1)	8.1 (1.5)	2.3
Land1	PM$_{10}$	16.1 (0.9)	6.7 (0.1)	1.6 (0.1)	8.7 (0.3)	0.6 (0.04)	1.7 (0.1)	64.6 (0.9)	1.0
Maeli2	PM$_{10}$	8.9 (1.2)	8.2 (0.2)	-	-	-	1.6 (0.1)	81.3(1.2)	0.9
MIR45	PM$_{10}$	3.6 (2.3)	3.6 (0.1)	-	-	-	1.1 (0.1)	91.7 (2.4)	0.8
D3	Sediments	13.0 (0.9)	11.1 (0.2)	-	-	-	-	75.9 (0.9)	1.0
H55	Sediments	46.1 (1.5)	29.7 (0.4)	6.5 (0.3)	1.3 (0.3)	-	1.2 (0.1)	15.2 (1.3)	3.8
Land1	Sediments	14.6 (1.1)	10.2 (0.3)	1.5 (0.2)	3.1 (0.2)	1.5 (0.1)	1.2 (0.1)	68.1 (1)	1.1
Maeli2	Sediments	9.3 (1.3)	7.1 (0.2)	-	-	-	1.4 (0.1)	82.2 (1.3)	0.8
MIR45	Sediments	4.3 (2)	4.1 (0.2)	-	-	-	1.7 (0.1)	89.9 (2)	0.8

Table 3: Estimated imaginary part of the volume average refractive index of Icelandic dust (PM_{10} fraction).

Samples	Assuming FeD = Hematite								Assuming FeD = Goethite							
	470 nm		520 nm		590 nm		660 nm		470 nm		520 nm		590 nm		660 nm	
	$\tilde{k}1$	$\tilde{k}2$	$\tilde{k}1$	$\tilde{k}2$	$\tilde{k}1$	$\tilde{k}2$	$\tilde{k}1$	$\tilde{k}2$	$\tilde{k}1$	$\tilde{k}2$	$\tilde{k}1$	$\tilde{k}2$	$\tilde{k}1$	$\tilde{k}2$	$\tilde{k}1$	$\tilde{k}2$
D3	0.010	0.002	0.009	0.002	0.008	0.002	0.007	0.002	0.010	0.002	0.009	0.002	0.008	0.002	0.007	0.003
H55	0.009	0.002	0.008	0.002	0.007	0.002	0.006	0.002	0.009	0.001	0.008	0.002	0.007	0.002	0.007	0.002
Land1	0.006	0.002	0.005	0.002	0.004	0.001	0.004	0.001	0.005	0.001	0.005	0.002	0.005	0.002	0.004	0.002
Maeli2	0.011	0.003	0.009	0.002	0.008	0.002	0.007	0.002	0.010	0.002	0.009	0.003	0.008	0.003	0.008	0.003
MIR45	0.006	0.001	0.006	0.001	0.005	0.001	0.004	0.002	0.006	0.001	0.006	0.001	0.005	0.002	0.004	0.002

Note: The $\tilde{\mathbf{k}}1$ and $\tilde{\mathbf{k}}2$ values are calculated using two different complex refractive indices for magnetite, from Huffman and Stapp (1973) and Querry (1985), respectively. If assuming FeD is purely hematite, the data shown in the table are calculated using the data from Longtin et al. (1988).

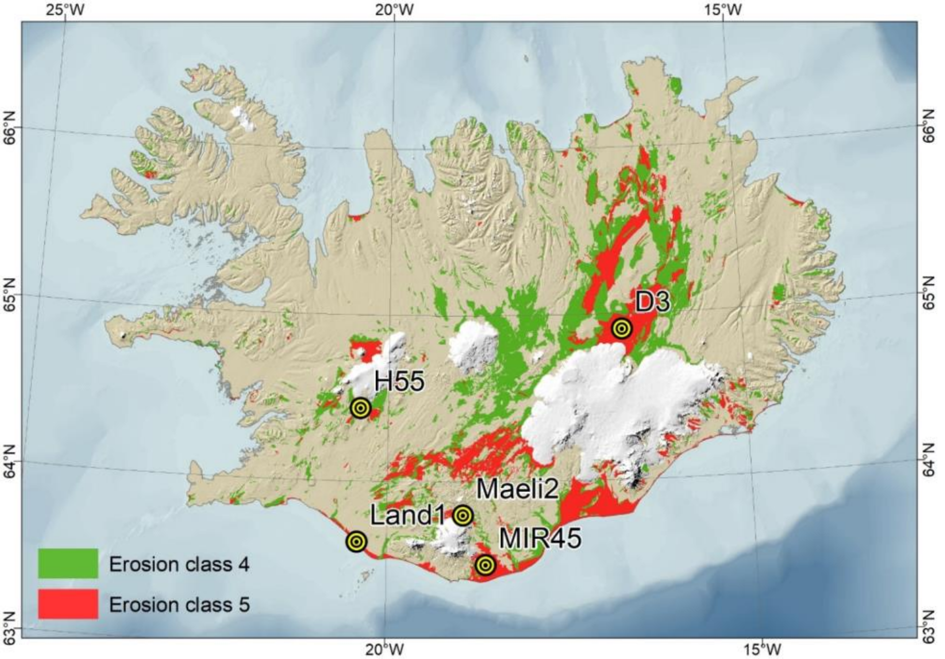

Figure 1: Surface sediment sampling sites and major dust hotspots. D3, Dyngjusandur hotspot; H55, Hagavatn hotspot; Land1, Landeyjarsandur; Maeli2, Mælifellssandur; MIR45, Myrdalssandur. In green, the unstable sandy areas. In red, the very unstable sandy areas. Note: Map prepared by Ólafur Arnalds using data created and owned by him at the Agricultural University of Iceland, older works (database housed by the Agricultural University of Iceland).

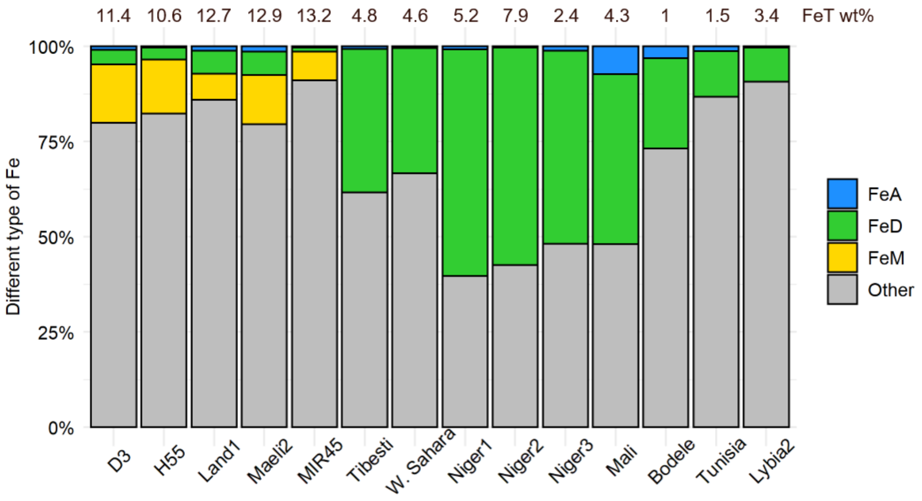

Figure 2: Percentages of ascorbate Fe (FeA), dithionite Fe (FeD), magnetite Fe (FeM) and other Fe to the total Fe (FeT) in Icelandic dust PM_{10} samples (this study) and African dust (Shi et al., 2011b). The data uncertainty was estimated using the error propagation formula: 12-22% FeA, 11-16% for FeD, 12-19% for FeM, ~11% for FeT. The original data are reported in Table S3 of the supporting information. Note that FeM was not measured in Shi et al. (2011b), but it is expected to be negligible in North African dust (Lazaro et al., 2008; Moskowitz et al., 2016).

955

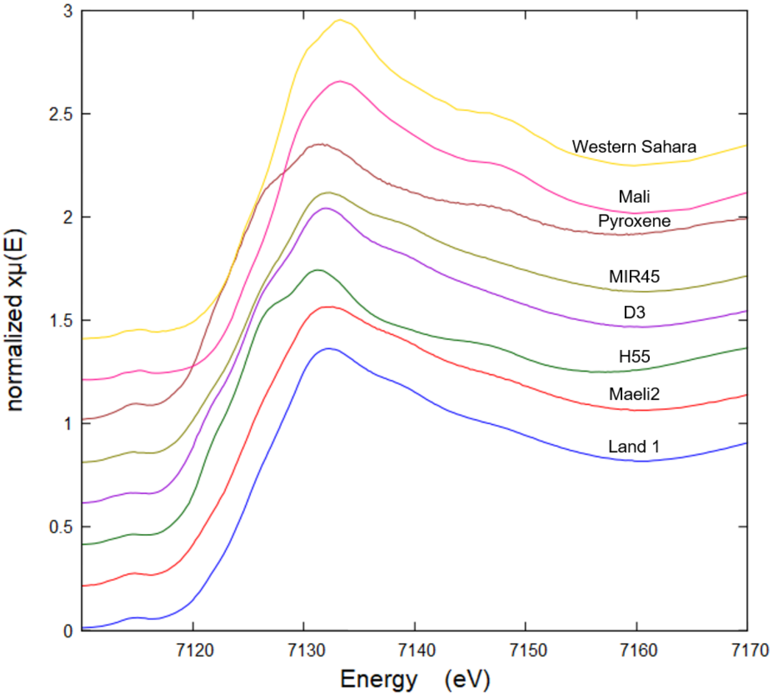

Figure 3: Fe Kedge XANES spectra of Icelandic Dust, natural pyroxene from Iceland, and African Dust. The Y-axis represents an arbitrary intensity.

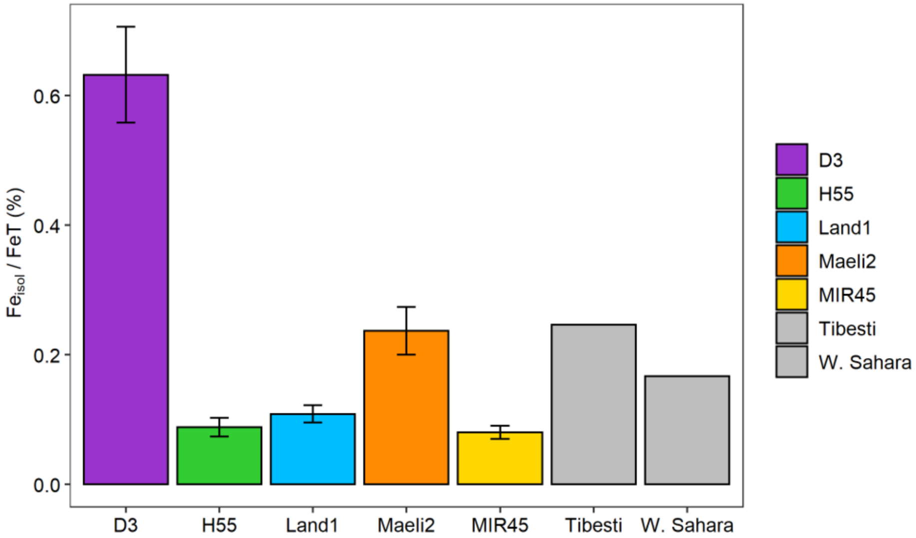

960

Figure 4: Initial Fe solubility (Fe$_{isol}$ / FeT, %) of Icelandic dust (this study). The data uncertainty was estimated using the error propagation formula. Data for African dust samples (Tibesti and W. Sahara) were from Shi et al. (2011c).

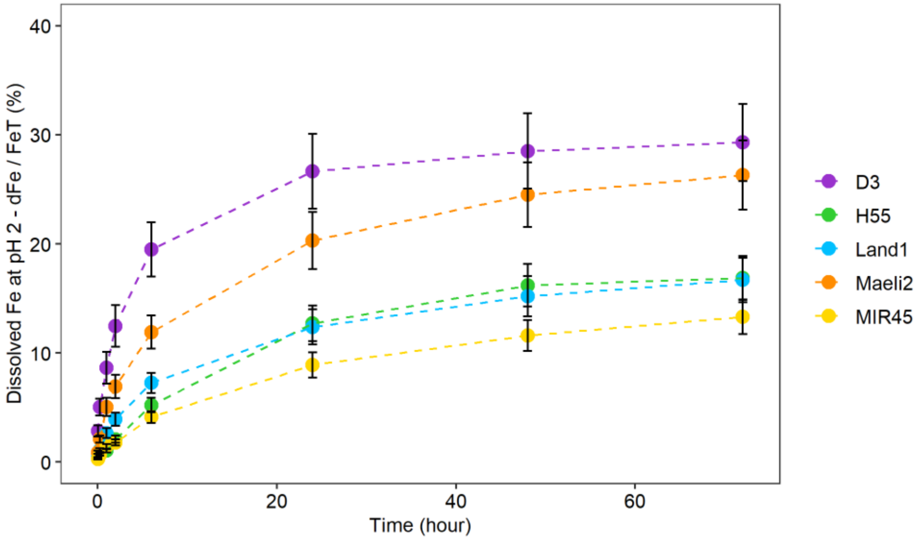

965 **Figure 5: Fe dissolution kinetics at pH 2. The data uncertainty was estimated using the error propagation formula.**

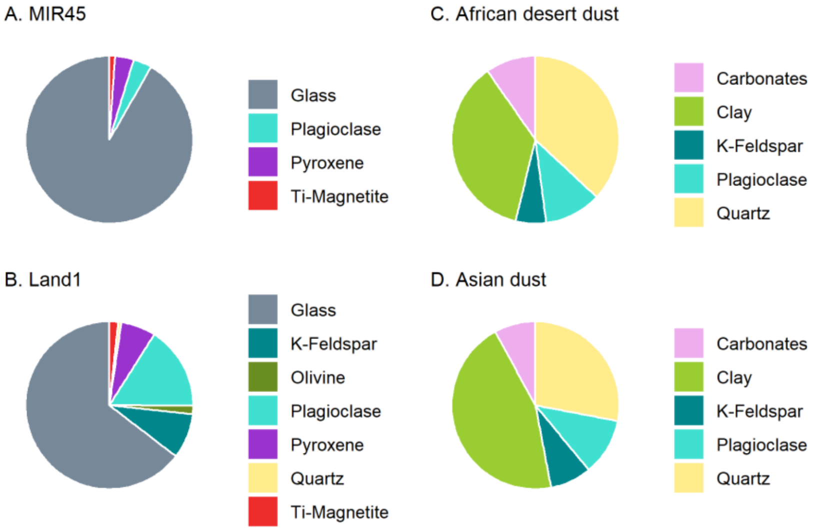

Figure 6: A-B. Mineralogy of Icelandic dust (MIR45 and Land1; PM_{10}). C. Mineral composition of North African desert dust (PM_{20}), representing the average bulk composition by X-ray diffraction of Tibesti, Western Sahara, Niger, and Mali samples (Shi et al., 2011b). D. Mineral composition of Asian dust (PM_{10}), average bulk composition by X-ray diffraction of dust from arid regions in Mongolia and North China collected in Seoul (Korea) during eight dust events in 2003-2005 (Jeong et al., 2008).

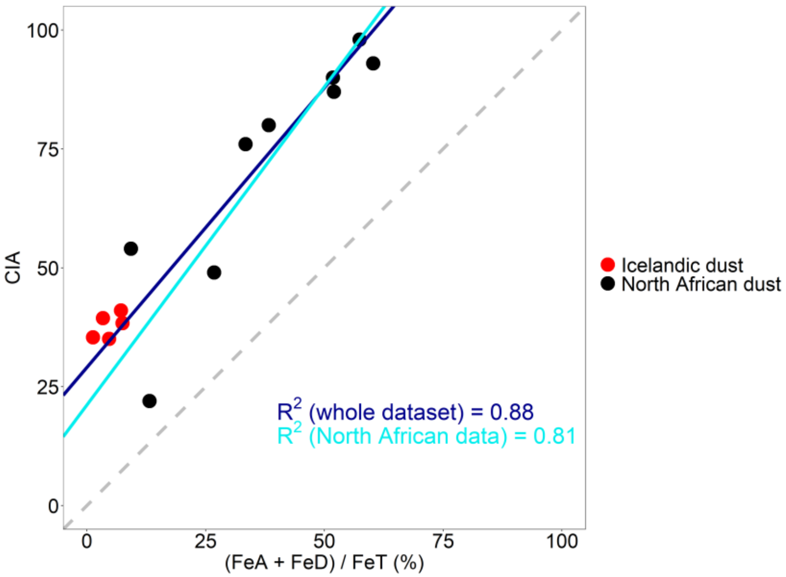

Figure 7: Correlation of the chemical index of alteration (CIA) with (FA + FeD) / FeT (%) performed using the standard major axis regression. Data for African dust are from Shi et al. (2011b). The regression line in blue was calculated including the whole dataset: Icelandic dust (this study) and North African dust (Shi et al., 2011b). The regression line in light blue was calculated using only the North African dust data (Shi et al., 2011b).

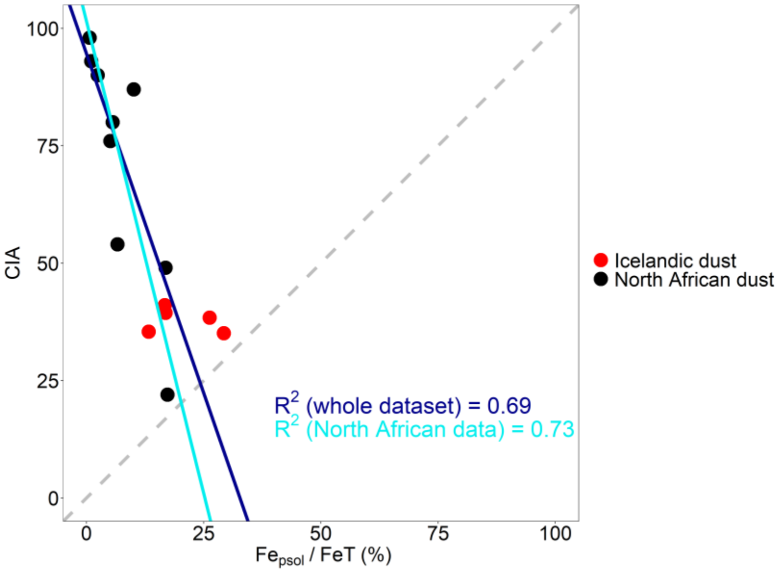

Figure 8: Correlation of the chemical index of alteration (CIA) with Fe$_{psol}$ / FeT (%) performed using the standard major axis regression. The regression line in blue was calculated including the whole dataset: Icelandic dust (this study) and North African dust (Shi et al., 2011b). The regression line in light blue was calculated using only the North African dust data (Shi et al., 2011b).